Journal of Computational Physics 504 (2024) 112886

Contents lists available at ScienceDirect

Journal of Computational Physics

journal homepage: www.elsevier.com/locate/jcp

A compact simple HWENO scheme with ADER time discretization for hyperbolic conservation laws I: Structured meshes ☆

Dongmi Luo [a], Shiyi Li [a], Jianxian Qiu [b], Jun Zhu [c], Yibing Chen [a,*]

[a] National Key Laboratory of Computational Physics, Institute of Applied Physics and Computational Mathematics, Beijing 100088, China
[b] School of Mathematical Sciences and Fujian Provincial Key Laboratory of Mathematical Modeling and High-Performance Scientific Computing, Xiamen University, Xiamen, Fujian 361005, China
[c] State Key Laboratory of Mechanics and Control of Mechanical Structures, Key Laboratory of Mathematical Modelling and High Performance Computing of Air Vehicles (NUAA), MIIT, Nanjing University of Aeronautics and Astronautics, Nanjing, Jiangsu 210016, PR China

ARTICLE INFO

Keywords:
Compact
High order
HWENO
Lax-Wendroff procedure
Hyperbolic conservation law

ABSTRACT

In this paper, a compact and high order ADER (Arbitrary high order using DERivatives) scheme using the simple HWENO method (ADER-SHWENO) is proposed for hyperbolic conservation laws. The newly-developed method employs the Lax-Wendroff procedure to convert time derivatives to spatial derivatives, which provides the time evolution of the variables at the cell interfaces. This information is required for the simple HWENO reconstructions, which take advantages of the simple WENO and the classic HWENO. Compared with the original Runge-Kutta HWENO method (RK-HWENO), the new method has two advantages. Firstly, RK-HWENO method must solve the additional equations for reconstructions, which is avoided for the new method. Secondly, the SHWENO reconstruction is performed once with one stencil and is different from the classic HWENO methods, in which both the function and its derivative values are reconstructed with two different stencils, respectively. Thus the new method is more efficient than the RK-HWENO method. Moreover, the new method is more compact than the existing ADER-WENO method. Besides, the new method makes the best use of the information in the ADER method. Thus, the time evolution of the cell averages of the derivatives is simpler than that developed in the work (Li et al. (2021) [17]). Numerical tests indicate that the new method can achieve high order for smooth solutions both in space and time, keep non-oscillatory at discontinuities.

1. Introduction

In this paper, we consider the numerical solutions of hyperbolic conservation laws. The major difficulty in solving nonlinear hyperbolic conservation laws is that the solution can develop discontinuities even if the initial condition is smooth. In the past decades, a large number of the high order finite volume methods have been developed to solve the equations, which can be divided for two groups. One is based on the cell averages, such as essentially non-oscillatory (ENO) [11], weighted ENO (WENO) [1,12] and

☆ The research is supported partly by National Key R&D Program of China (Grant Number 2022YFA1004500), National Natural Science Foundation of China (Grant Nos. 12101063, 12071392, 12271052), Grant No. MCMS-I-0120G01.

* Corresponding author.
E-mail addresses: dongmiluo@stu.xmu.edu.cn (D. Luo), lishiyi14@tsinghua.org.cn (S. Li), jxqiu@xmu.edu.cn (J. Qiu), zhujun@nuaa.edu.cn (J. Zhu), chen_yibing@iapcm.ac.cn (Y. Chen).

https://doi.org/10.1016/j.jcp.2024.112886
Received 9 April 2023; Received in revised form 9 January 2024; Accepted 24 February 2024

Available online 29 February 2024

so on. However, the stencil used for the reconstructions is becoming wider with an increasing the order of accuracy. The other group is discontinuous Galerkin method (DG) [2,3,19], Hermite WENO (HWENO) [20,22,23,37,40] and so on, which are compact methods. Generally, these methods should solve the additional equations to obtain the internal freedom for the reconstructions, which is used to time evolution.

Although these methods are arbitrarily high order in space. Most of them are discretized with Runge-Kutta (RK) methods in time. For the multi-stage methods, the reconstruction needs to be performed several times per time step. To avoid the disadvantages of the multi-stage temporal discretization methods, lots of high order one-stage methods such GRP (the generalized Riemann problem) [30], HGKS (high order gas kinetic scheme) [17,18,26], ADER (Arbitrary high order using DERivatives) approach of Toro et al. [28,29,31], and other Lax-Wendroff procedure based methods [21,24,25] are proposed.

In the past years, the gas-kinetic scheme (GKS) has been developed systematically [16–18,26]. HGKS has been proposed without employing RK time discretization [18,26]. Moreover, a compact and efficient HGKS (CEHGKS) [17] is proposed for the hyperbolic conservation laws recently, which is based on the framework of a one-stage efficient HGKS and can achieve high order accuracy both in space and time. The numerical examples [17] show the effectiveness of CEHGKS. However, the technique is only suitable in the framework of HGKS.

Another popular one-stage temporal discretization method is ADER method, which was first put forward by Toro and collaborators for linear problems on Cartesian meshes [33]. Soon after that the ADER methods are extended to many nonlinear problems. ADER methods are combined with WENO methodology (ADER-WENO) to obtain the non-oscillatory of very high order of accuracy in space and time for nonlinear hyperbolic conservation laws [6,7,10,28,29,31]. Similar to the traditional RK-WENO, the stencil used in ADER-WENO reconstructions is becoming wider with an increasing the order of accuracy, which makes the method more complex on high dimension and unstructured meshes. To avoid the disadvantages of ADER-WENO methods, the ADER approaches are extended to nonlinear systems in the framework of DG methods (ADER-DG) [5,8]. However, ADER-DG methods also need to solve the additional equations for obtaining the internal freedom for reconstructions and time advancing, which increases the computational costs.

Motivated by the CEHGKS and ADER methods, a compact and high order ADER scheme using the simple HWENO (SHWENO) method for hyperbolic conservation laws is proposed in this paper, which is denoted by ADER-SHWENO. The method is based on a fundamental assumption, i.e., all the variables of the equations are smooth within a space-time computational cell, which is also used for the work [17] and a reason why the method [17] can succeed indeed. Thus the Lax-Wendroff procedure can be employed to convert time derivatives to spatial derivatives, which provides the time evolution of the variables at the cell interfaces. This information is required for the SHWENO reconstructions, which combine the ideas of the simple WENO [38,39] and classic HWENO [22,23,40]. Note that the classic HWENO [22,23,40] must solve the additional equation for time evolution, which is avoided for the new method. Moreover, the SHWENO reconstruction is performed once with one stencil and is different from the classic HWENO methods [22,23,40], in which both the function and its derivative values are reconstructed with two different stencils, respectively. Thus ADER-SHWENO is more efficient than the classic HWENO methods. Moreover, the new method makes the best use of the information in the ADER method. Therefore, the time evolution of the cell averages of the solutions is simpler than that in the work [17], where it includes the non-equilibrium and equilibrium parts, which need to be computed additionally and increase the computational cost. Besides, the approximation to leading term is rth order accuracy for the rth ADER-SHWENO method while $(2r-1)$th order accuracy for rth order ADER-WENO method [28]. Therefore, the newly-developed ADER-SHWENO method is more compact than ADER-WENO method [28]. Finally, an efficient and compact fifth order one-stage method is developed by combining ADER and SHWENO reconstructions. Numerical tests show that the new method can achieve high order for smooth solutions both in space and time, keep non-oscillatory at discontinuities.

An outline of the paper is given as follows. The ADER scheme based on the simple HWENO method is described in Section 2 and Section 3 for one and two dimensional hyperbolic conservation laws in detail, respectively. In Section 4, the algorithm of the method is presented briefly. One and two dimensional numerical examples are presented to demonstrate the accuracy and the capability of the ADER-SHWENO method in Section 5. In Section 6, conclusions are drawn.

2. The numerical scheme in one dimension

In this section, we describe the ADER-SHWENO method for the numerical solution of hyperbolic conservation laws on a uniform mesh. We consider the conservation law in one dimension in the form

$$\begin{cases} W_t + F(W)_x = 0, \\ W(x,0) = W_0(x), \end{cases} \tag{2.1}$$

where W and $F(W)$ are either scalars or vectors.

Assume the computational domain Ω is divided into N nonoverlapping cells $\{I_j = (x_{j-\frac{1}{2}}, x_{j+\frac{1}{2}}), j = 1, \cdots, N\}$, $\Delta x = x_{j+\frac{1}{2}} - x_{j-\frac{1}{2}}$, and $x_j = \frac{1}{2}(x_{j+\frac{1}{2}} + x_{j-\frac{1}{2}})$. Assume the computational time is T and $0 = t_0 < t_1 < \cdots < t_n < t_{n+1} < \cdots \le T$. Integrating (2.1) on $I_j \times (t_n, t_{n+1})$ yields

$$\bar{W}(x_j, t_{n+1}) = \bar{W}(x_j, t_n) - \frac{\Delta t}{\Delta x}\Big(\frac{1}{\Delta t}\int_{t_n}^{t_{n+1}} F(x_{j+\frac{1}{2}}, t)dt - \frac{1}{\Delta t}\int_{t_n}^{t_{n+1}} F(x_{j-\frac{1}{2}}, t)dt\Big),$$

where $\bar{W}(x_j,t_n)=\frac{1}{\Delta x}\int_{I_j}W(x,t_n)dx$ is the cell average in cell I_j at time t_n, and $\Delta t=t_{n+1}-t_n$. Thus, the finite volume method for the equation is defined as

$$\bar{W}_j^{n+1}=\bar{W}_j^n-\frac{\Delta t}{\Delta x}(\hat{F}_{j+\frac{1}{2}}-\hat{F}_{j-\frac{1}{2}}), \tag{2.2}$$

where $\bar{W}_j^n$ is a high order approximation to $\bar{W}(x_j,t_n)$, and $\hat{F}_{j+\frac{1}{2}}\approx\frac{1}{\Delta t}\int_{t_n}^{t_{n+1}}F(x_{j+\frac{1}{2}},t)dt$ is the numerical flux, which is also a high order approximation to the physical flux. For the traditional finite volume methods, an explicit and the third order TVD Runge-Kutta scheme [27] is used for temporal discretization. In order to obtain the arbitrary order of accuracy in both time and space, the ADER approach [28] is employed in this paper. The ADER approach mainly contains three steps [28]:

1. first reconstruct the high order point-wise values from the cell averages;
2. after the reconstruction, solve the generalized Riemann problem at the cell interface;
3. finally evaluate the numerical flux in the conservative scheme (2.2).

2.1. The generalized Riemann problem

In this section, we describe the generalized Riemann problem. We assume the point-wise values of the conservative variables have been reconstructed, which are represented by the vector polynomials $p_j(x), j=1,\cdots,N$. Then at each cell interface, the generalized Riemann problem (GRP) with the reconstruction polynomials is proposed [28,29]:

$$\begin{aligned}&\partial_t W+\partial_x F(W)=0\\&W(x,0)=\begin{cases}W_L(x)=p_j(x), & x<x_{j+\frac{1}{2}},\\ W_R(x)=p_{j+1}(x), & x>x_{j+\frac{1}{2}},\end{cases}\end{aligned} \tag{2.3}$$

which is different from the conventional piece-wise constant data Riemann problem. Now the solution no longer contains regions of constant values and characteristics are curved lines. Thus, we need to find an approximate solution for the interface state $W(x_{j+\frac{1}{2}},\tau)$, where τ is local time $\tau=t-t_n$ using the method developed in [30]. The approximate solution $W(x_{j+\frac{1}{2}},\tau)$ can be evaluated by a Taylor expansion of the interface state in time

$$W(x_{j+\frac{1}{2}},\tau)\approx W(x_{j+\frac{1}{2}},0^+)+\sum_{k=1}^{4}[\partial_t^{(k)}W(x_{j+\frac{1}{2}},0^+)]\frac{\tau^k}{k!}, \tag{2.4}$$

where

$$\partial_t^{(k)}W(x,t)=\frac{\partial^k}{\partial t^k}W(x,t),\quad 0^+\equiv\lim_{\tau\to 0^+}\tau.$$

(2.4) implies the solution is smooth in time. From (2.4), one can observe that the approximate solution contains two parts: a leading term $W(x_{j+\frac{1}{2}},0^+)$ and the high order terms with coefficients determined by the temporal derivatives $\partial_t^{(k)}W(x_{j+\frac{1}{2}},0^+)$. Thus, the values of a leading term and high order terms at the cell interfaces need to be evaluated, which are described in the following sections.

2.1.1. The leading term

The leading term $W(x_{j+\frac{1}{2}},0^+)$ accounts for the interaction of the boundary extrapolated values $W_L(x_{j+\frac{1}{2}})$ and $W_R(x_{j+\frac{1}{2}})$, which are taken to be the Godunov state of the conventional Riemann problem:

$$\begin{aligned}&\partial_t W+\partial_x F(W)=0\\&W(x,0)=\begin{cases}W_L(x_{j+\frac{1}{2}}), & x<x_{j+\frac{1}{2}},\\ W_R(x_{j+\frac{1}{2}}), & x>x_{j+\frac{1}{2}}.\end{cases}\end{aligned} \tag{2.5}$$

The leading term is obtained by solving the above equation. In this paper, $W_L(x_{j+\frac{1}{2}})$ and $W_R(x_{j+\frac{1}{2}})$ are directly obtained by the SHWENO reconstruction in Sec. 2.3. For scalar cases, we solve the Riemann problem exactly. For the Euler systems, the HLLC Riemann solver [30] is adopted, which contains all waves in the Riemann problem solution.

2.1.2. The high order term

To compute the high order terms in (2.4) we need to compute the coefficients, which are the partial derivatives $\partial_t^{(k)}W(x_{j+\frac{1}{2}},0^+)$ at $x=x_{j+\frac{1}{2}},t=0$. Thus, the high order terms are evaluated in two steps.

First, we express all time derivatives as functions of space derivatives by the Lax-Wendroff procedure. For systems the procedure yields the following expressions:

$$\partial_t W=-\frac{\partial F}{\partial W}\partial_x W,$$

$$\partial_{tx}W = -(\frac{\partial^2 F}{\partial W^2}\partial_x W)\partial_x W - \frac{\partial F}{\partial W}\partial_{xx}W,$$
$$\partial_{tt}W = -(\frac{\partial^2 F}{\partial W^2}\partial_t W)\partial_x W - \frac{\partial F}{\partial W}\partial_{xt}W, \tag{2.6}$$

and so on. In practice, it is more convenient to implement (2.6) in componentwise manner rather than in the matrix form.

Then differentiating the governing equation (2.1) with respect to x, we obtain

$$\partial_t W^{(k)} + A(W)\partial_x W^{(k)} = H(W, W^{(1)}, W^{(2)}, \cdots, W^{(k-1)}), \tag{2.7}$$

where $W^{(k)} = \frac{\partial^k}{\partial x^k}W, 1 \le k \le 4$, $A(W)$ is the Jacobian matrix, H is a nonlinear source term depending on derivatives of lower order as well as $W(x,t)$ itself. However, it is not easy to solve these nonlinear inhomogeneous problems. For simplicity, we neglect the source terms H which comes into effect for $\tau > 0$ only. Additionally, we linearize the equation around the leading term $W(x_{j+\frac{1}{2}}, 0^+)$ of the time expansion (2.4) and replace the piece-wise polynomial initial data by left and right boundary extrapolated values of spatial derivatives at $x_{j+\frac{1}{2}}$. Then high order terms are obtained by solving the following linearized Riemann problem [28,31]:

$$\partial_t W^{(k)} + A_{j+\frac{1}{2}}\partial_x W^{(k)} = 0$$
$$W^{(k)}(x,0) = \begin{cases} \partial_x^{(k)} W_L(x_{j+\frac{1}{2}}), & x < x_{j+\frac{1}{2}}, \\ \partial_x^{(k)} W_R(x_{j+\frac{1}{2}}), & x > x_{j+\frac{1}{2}}, \end{cases} \tag{2.8}$$

where $A_{j+\frac{1}{2}} = F'(W(x_{j+\frac{1}{2}}, 0^+))$ is the Jacobian matrix.

Note that the coefficient matrix $A_{j+\frac{1}{2}}$ is the same for all spatial derivatives $W^{(k)}$ and is evaluated only once, using the leading term of the expansion. The initial condition for (2.8) is found directly by differentiating the given SHWENO reconstruction polynomial with respect to x. In the paper, we use the same linear weights and smoothness indicators for the function and for all derivatives. Then the linear Riemann problem (2.8) can be solved directly.

2.2. The evaluation of the numerical flux

Finally, having computed all spatial derivatives we form the Tayor expansion (2.4). There exist two options to evaluate the numerical flux [29]. In the paper, the state-expansion ADER [28] is employed, in which the approximate state (2.4) is inserted into the definition of the numerical flux (2.2). To evaluate the numerical flux an appropriate Gaussian rule is used:

$$\hat{F}_{j+\frac{1}{2}} = \sum_{\alpha=0}^{K_\alpha} F(W(x_{j+\frac{1}{2}}, \lambda_\alpha \Delta t))w_\alpha, \tag{2.9}$$

where λ_α and w_α are properly scaled nodes and weights of the rule, and K_α is the number of the nodes.

2.3. SHWENO reconstruction in one dimension

In the previous sections, the GRP and evaluation of the flux are presented. Recall that we assume the polynomials are reconstructed. In this subsection, the simple HWENO reconstruction is given. For the traditional ADER methods, both WENO and DG methods are applied for reconstructions. For the classic WENO method [12], the approximation to the leading term is $(2r-1)$th order accuracy for rth order ADER method. Thus, the stencil used in reconstructions is becoming wider with an increasing order of accuracy. On the other hand, for DG method [2,3], the additional equations need to be solved to obtain the internal freedom for reconstruction and time advancing, which increases the computational costs. To avoid the disadvantages of WENO and DG method, the simple HWENO method [17] is employed in this paper. The reconstruction method combines the ideas of the simple WENO and the classic HWENO method. Thus the linear weights can be chosen arbitrary positive numbers except that its sum equal to one and the cell averages as well as the cell averages of the derivatives are needed for reconstruction. The procedure is the same as the work [17]. Assume

$$\bar{V}_j = \frac{1}{\Delta x}\int_{I_j} W_x(x,t)dx, \tag{2.10}$$

which is the cell average of the derivatives of the solution. Then the reconstruction of the simple HWENO from the cell averages $\{\bar{W}_j, \bar{V}_j\}$ is described in the following in detail.

Step 1. Define a series of polynomials of different degrees.

Step 1.1. Similar to the work in [17,22], choose the big stencil $T_1 = \{I_{j-1}, I_j, I_{j+1}\}$. Then a quartic polynomial $P_1(x)$ based on the cell averages of the solution and its derivative is constructed, which satisfies

$$\frac{1}{\Delta x}\int_{I_l} P_1(x)dx = \bar{W}_l,\ l = j-1, j, j+1,$$

$$\frac{1}{\Delta x}\int_{I_l}\frac{dP_1(x)}{dx}dx=\bar{V}_l,\ l=j-1,j+1.$$

Step 1.2. Choose the other two smaller stencils $T_2=\{I_{j-1},I_j\}$ and $T_3=\{I_j,I_{j+1}\}$ to construct two linear polynomials $P_2(x)$ and $P_3(x)$, which satisfy

$$\frac{1}{\Delta x}\int_{I_l}P_2(x)dx=\bar{W}_l,\ l=j-1,j,$$

and

$$\frac{1}{\Delta x}\int_{I_l}P_3(x)dx=\bar{W}_l,\ l=j,j+1,$$

respectively.

Step 2. Similar to the work in [14,15,39], we rewrite $P_1(x)$ as:

$$P_1(x)=\gamma_1(\frac{1}{\gamma_1}P_1(x)-\frac{\gamma_2}{\gamma_1}P_2(x)-\frac{\gamma_3}{\gamma_1}P_3(x))+\gamma_2P_2(x)+\gamma_3P_3(x). \tag{2.11}$$

Note that the equation (2.11) holds true for any γ_1,γ_2 and γ_3 with $\gamma_1\neq 0$. Here, γ_1,γ_2 and γ_3 are taken as the linear weights. There is no requirement on the values of these linear weights for accuracy besides $\gamma_1+\gamma_2+\gamma_3=1$. The choice of these linear weights is solely based on the balance between accuracy and ability to achieve essentially non-oscillation property. In this paper, we set the linear weights as follows: $\gamma_1=0.994,\gamma_2=0.003$ and $\gamma_3=0.003$.

Step 3. The smoothness indicators, denoted by $\beta_l,\ l=1,2,3$ are computed [12] as

$$\beta_l=\sum_{s=1}^{k}\int_{I_j}\Delta x^{2s-1}(\frac{d^sP_l(x)}{dx^s})^2dx,\quad l=1,2,3,$$

where $k=4$ for $l=1$ and $k=1$ for $l=2,3$. They measure how smooth the function $P_l(x)$ is in the target cell I_j.

Step 4. Compute the nonlinear weights based on the linear weights and smoothness indicators

$$\omega_l=\frac{\bar{\omega}_l}{\bar{\omega}_1+\bar{\omega}_2+\bar{\omega}_3},\ \bar{\omega}_s=\gamma_s(1+\frac{\kappa}{\epsilon+\beta_s}),l=1,2,3;s=1,2,3, \tag{2.12}$$

where $\kappa=\frac{1}{4}(|\beta_1-\beta_2|+|\beta_1-\beta_3|)^2$, and ϵ is a small positive number to avoid the denominator to become zeros, which is set to be 10^{-6} in all the computations in this work.

Step 5. Replace the linear weights (2.11) with the nonlinear weights (2.12), and the final HWENO reconstruction of the conservative values at the point $x_{j+\frac{1}{2}}$ on the cell I_j is given by

$$W^-_{j+\frac{1}{2}}=\omega_1(\frac{1}{\gamma_1}P_1(x_{j+\frac{1}{2}})-\frac{\gamma_2}{\gamma_1}P_2(x_{j+\frac{1}{2}})-\frac{\gamma_3}{\gamma_1}P_3(x_{j+\frac{1}{2}}))+\omega_2P_2(x_{j+\frac{1}{2}})+\omega_3P_3(x_{j+\frac{1}{2}}). \tag{2.13}$$

The reconstruction to $W^+_{j+\frac{1}{2}}$ is mirror symmetric with respect to x_j of the above procedure.

2.4. The evaluation of the cell average of W_x

Note that in Sec. 2.3 the cell averages of W_x are needed for the SHWENO reconstruction in the next time step, which is evaluated in the following.

From (2.10), at time t_{n+1} we have

$$\bar{V}_j^{n+1}=\frac{1}{\Delta x}\int_{I_j}W_x(x,t_{n+1})dx=\frac{W(x_{j+\frac{1}{2}},t_{n+1})-W(x_{j-\frac{1}{2}},t_{n+1})}{\Delta x}. \tag{2.14}$$

In the classic HWENO method [22], an additional equation with respect to the cell average of W_x is solved for time evolution. To avoid the disadvantages of HWENO methods, Li et al. [17] employed the equation (2.14) and evaluated the value of $W(x_{j+\frac{1}{2}},t_{n+1})$ in the framework of GKS, which includes the non-equilibrium and equilibrium states. Thus these terms should be evaluated in order to calculate $W(x_{j+\frac{1}{2}},t_{n+1})$, which increases the complexity of the method developed in [17].

Recall the ADER method described in the previous section. From (2.9), one can see that the numerical solutions at the different times between t_n and t_{n+1} should be computed for the numerical flux. In the ADER method, the solutions at different times are evaluated by a Taylor expansion of the interface state in time, i.e. (2.4). Motivated by that, a fifth order approximation of $W(x_{j+\frac{1}{2}},t_{n+1})$ can be evaluated by

$$W(x_{j+\frac{1}{2}},t_n+\Delta t)\approx W(x_{j+\frac{1}{2}},t_n^+)+\sum_{k=1}^{4}[\partial_t^{(k)}W(x_{j+\frac{1}{2}},t_n^+)]\frac{(\Delta t)^k}{k!}, \tag{2.15}$$

which implies the solution in time is smooth.

In fact, the leading term $W(x_{j+\frac{1}{2}},t_n^+)$ and high order term $\partial_t^{(k)}W(x_{j+\frac{1}{2}},t_n^+)$ have been evaluated in the ADER method, which can be used directly in (2.15). Therefore, the evaluation of $W(x_{j+\frac{1}{2}},t_{n+1})$ in our new method almost does not introduce the additional computational cost and is simpler than that in the work [17]. Finally, we can obtain the cell averages of W_x at the next time using (2.14).

Remark 1. From the procedure above, one can see that we only need to take $\tau=\Delta t$ in (2.4) to get (2.15) for updating the cell average of W_x. In addition, the leading term and high order term are evaluated in ADER method. Therefore, we almost directly use trivial work to update the cell average of W_x using (2.14). This is the key point of our method.

Remark 2. In the practical implementations, we can use the Gauss-Lobatto quadrature rule in (2.9), which includes the values at both ends, i.e. t_n and t_{n+1}. Thus, we can further reduce the computational cost.

3. The numerical scheme in two dimensions

In this section, we describe the ADER-SHWENO method for two dimensional problems. We consider the form

$$\begin{cases} W_t+F(W)_x+G(W)_y=0,\\ W(x,y,0)=W_0(x,y), \end{cases} \tag{3.1}$$

where W, $F(W)$ and $G(W)$ are either scalars or vectors. We use a rectangle mesh of cell size Δx and Δy in x and y directions, respectively. We denote the cells by

$$I_{ij}=(x_{i-\frac{1}{2}},x_{i+\frac{1}{2}})\times(y_{j-\frac{1}{2}},y_{j+\frac{1}{2}}),$$

where $x_{i+\frac{1}{2}}=\frac{1}{2}(x_i+x_{i+1}), y_{j+\frac{1}{2}}=\frac{1}{2}(y_j+y_{j+1})$.

Integrating (3.1) on $I_{ij}\times(t_n,t_{n+1})$, we obtain

$$\bar{W}(x_i,y_j,t_{n+1})=\bar{W}(x_i,y_j,t_n)-\frac{\Delta t}{\Delta x\Delta y}[\frac{1}{\Delta t}\int_{t_n}^{t_{n+1}}\int_{y_{j-\frac{1}{2}}}^{y_{j+\frac{1}{2}}}F(W(x_{i+\frac{1}{2}},y,t))-F(W(x_{i-\frac{1}{2}},y,t))dydt]-$$

$$\frac{\Delta t}{\Delta x\Delta y}[\frac{1}{\Delta t}\int_{t_n}^{t_{n+1}}\int_{x_{i-\frac{1}{2}}}^{x_{i+\frac{1}{2}}}G(W(x,y_{j+\frac{1}{2}},t))-G(W(x,y_{j-\frac{1}{2}},t))dxdt],$$

where $\bar{W}(x_i,y_j,t_n)=\frac{1}{\Delta x\Delta y}\int_{I_{ij}}W(x,y,t_n)dxdy$. Then the finite volume method in two dimensions is given by

$$\bar{W}_{ij}^{n+1}=\bar{W}_{ij}^{n}-\frac{\Delta t}{\Delta x\Delta y}(\hat{F}_{i+\frac{1}{2},j}-\hat{F}_{i-\frac{1}{2},j})-\frac{\Delta t}{\Delta x\Delta y}(\hat{G}_{i,j+\frac{1}{2}}-\hat{G}_{i,j-\frac{1}{2}}), \tag{3.2}$$

where $\hat{F}_{i+\frac{1}{2},j}\approx\frac{1}{\Delta t}\int_{t_n}^{t_{n+1}}\int_{y_{j-\frac{1}{2}}}^{y_{j+\frac{1}{2}}}F(W(x_{i+\frac{1}{2}},y,t))dydt, \hat{G}_{i,j+\frac{1}{2}}\approx\frac{1}{\Delta t}\int_{t_n}^{t_{n+1}}\int_{x_{i-\frac{1}{2}}}^{x_{i+\frac{1}{2}}}G(W(x,y_{j+\frac{1}{2}},t))dxdt$. One can observe that this leads to equations including the line integrals on the cell I_{ij}, which can be computed by the Gaussian quadrature rule

$$\hat{F}_{i+\frac{1}{2},j}=\sum_{G_y}\Delta y w_{G_y}(\frac{1}{\Delta t}\int_{t_n}^{t_{n+1}}F(W(x_{i+\frac{1}{2}},y_{G_y},t))dt), \tag{3.3}$$

$$\hat{G}_{i,j+\frac{1}{2}}=\sum_{G_x}\Delta x w_{G_x}(\frac{1}{\Delta t}\int_{t_n}^{t_{n+1}}G(W(x_{G_x},y_{i+\frac{1}{2}},t))dt), \tag{3.4}$$

where x_{G_x} and y_{G_y} are the Gaussian points on $(x_{i-\frac{1}{2}},x_{i+\frac{1}{2}})$ and $(y_{j-\frac{1}{2}},y_{j+\frac{1}{2}})$, respectively. w_{G_x} and w_{G_y} are the corresponding weights. As one dimensional case, we should evaluate the numerical fluxes (3.3) and (3.4). Here we concentrate on $\hat{F}_{i+\frac{1}{2},j}$ and the other one $\hat{G}_{i,j+\frac{1}{2}}$ is obtained in a similar manner.

3.1. The generalized Riemann problem in two dimensions

After the reconstruction is carried out for each Gaussian integration point $(x_{i+\frac{1}{2}}, y_{G_y})$ at the cell interface, the generalized Riemann problem (2.3) can be proposed along the x-direction. Then we can obtain a high order approximation to $W(x_{i+\frac{1}{2}}, y_{G_y}, \tau)$. All steps of the solution procedure are the same as in the one dimensional case. The Taylor series expansion in time is written as following:

$$W(x_{i+\frac{1}{2}}, y_{G_y}, \tau) = W(x_{i+\frac{1}{2}}, y_{G_y}, 0^+) + \sum_{k=1}^{4} [\partial_t^{(k)} W(x_{j+\frac{1}{2}}, y_{G_y}, 0^+)] \frac{\tau^k}{k!}. \tag{3.5}$$

The leading term $W(x_{i+\frac{1}{2}}, y_{G_y}, 0^+)$ is the Godunov state of the conventional Riemann problem:

$$\begin{aligned} &\partial_t W + \partial_x F(W) = 0 \\ &W(x,0) = \begin{cases} W_L(x_{i+\frac{1}{2}}, y_{G_y}), & x < x_{i+\frac{1}{2}}, \\ W_R(x_{i+\frac{1}{2}}, y_{G_y}), & x > x_{i+\frac{1}{2}}, \end{cases} \end{aligned} \tag{3.6}$$

which can be solved by an exact or HLLC Riemann solver. To evaluate the high order term we first use the Lax-Wendroff procedure to express the time derivatives as functions of space derivatives. Then we can obtain

$$\begin{aligned} \partial_t W &= -(\frac{\partial F}{\partial W})\partial_x W - (\frac{\partial G}{\partial W})\partial_y W, \\ \partial_{tx} W &= -(\frac{\partial^2 F}{\partial W^2}\partial_x W)(\partial_x W) - (\frac{\partial F}{\partial W})\partial_{xx} W - (\frac{\partial^2 G}{\partial W^2}\partial_x W)(\partial_y W) - (\frac{\partial G}{\partial W})\partial_{xy} W, \\ \partial_{ty} W &= -(\frac{\partial^2 F}{\partial W^2}\partial_y W)(\partial_x W) - (\frac{\partial F}{\partial W})\partial_{xy} W - (\frac{\partial^2 G}{\partial W^2}\partial_y W)(\partial_y W) - (\frac{\partial G}{\partial W})\partial_{yy} W, \\ \partial_{tt} W &= -(\frac{\partial^2 F}{\partial W^2}\partial_t W)(\partial_x W) - (\frac{\partial F}{\partial W})\partial_{tx} W - (\frac{\partial^2 G}{\partial W^2}\partial_t W)(\partial_y W) - (\frac{\partial G}{\partial W})\partial_{ty} W, \end{aligned}$$

and so on. These equations can be also used for systems. However, $\frac{\partial F}{\partial W}$ is a matrix and $\frac{\partial^2 F}{\partial W^2}$ is a three-dimensional tensor, etc. After getting the expression, the high order terms are obtained by solving the linearized Riemann problem:

$$\begin{aligned} &\partial_t W^{(m+n)} + A_{i+\frac{1}{2},j}\partial_x W^{(m+n)} = 0 \\ &W^{(m+n)}(x, y_{G_y}, 0) = \begin{cases} \partial_{x^m y^n}^{(m+n)} W_L(x_{i+\frac{1}{2}}, y_{G_y}), & x < x_{i+\frac{1}{2}}, \\ \partial_{x^m y^n}^{(m+n)} W_R(x_{i+\frac{1}{2}}, y_{G_y}), & x > x_{i+\frac{1}{2}}, \end{cases} \end{aligned} \tag{3.7}$$

where $W^{(m+n)} = \frac{\partial^{m+n}}{\partial x^m \partial y^n} W = \partial_{x^m y^n}^{(m+n)} W$, $1 \le m+n \le 4$ and $A_{i+\frac{1}{2},j} = F'(W(x_{i+\frac{1}{2}}, y_{G_y}, 0^+))$. Then the Taylor expansion (3.5) can be formed for the interface state at the Gaussian point $(x_{i+\frac{1}{2}}, y_{G_y})$. Finally the numerical flux can be evaluated by

$$\hat{F}_{i+\frac{1}{2},j} = \sum_{G_y} \Delta y w_{G_y} \sum_{\alpha=0}^{K_\alpha} F(W(x_{i+\frac{1}{2}}, y_{G_y}, \lambda_\alpha \Delta t)) w_\alpha. \tag{3.8}$$

3.2. SHWENO reconstruction in two dimensions

For SHWENO reconstruction on Cartesian meshes, one can employ either a direct two dimensional procedure or a dimension-by-dimension strategy [20]. In this paper, the dimension-by-dimension strategy is adopted. To perform the reconstruction, the cell averages of W, W_x, W_y and W_{xy} are denoted by

$$\begin{aligned} \Delta x \Delta y \bar{W}_{ij} &= \int_{I_{ij}} W dx dy, \\ \Delta x \Delta y \bar{V}_{ij} &= \int_{I_{ij}} W_x dx dy, \\ \Delta x \Delta y \bar{Y}_{ij} &= \int_{I_{ij}} W_y dx dy, \\ \Delta x \Delta y \bar{Z}_{ij} &= \int_{I_{ij}} W_{xy} dx dy. \end{aligned} \tag{3.9}$$

The reconstruction is as follows. First, we perform two y-direction reconstructions as Sec. 2.3, i.e.,

$$\begin{aligned} \{\bar{W}_{mn}, \bar{Y}_{mn}\} &\to \bar{W}_{i+l,j}(y_{G_y}) \approx \frac{1}{\Delta x} \int\limits_{I_{i+l,j}} W(x, y_{G_y}) dx, \\ \{\bar{V}_{mn}, \bar{Z}_{mn}\} &\to \bar{W}_{x,i+l,j}(y_{G_y}) \approx \frac{1}{\Delta x} \int\limits_{I_{i+l,j}} W_x(x, y_{G_y}) dx. \end{aligned}$$

Then we use $\bar{W}_{i+l,j}(y_{G_y})$ and $\bar{W}_{x,i+l,j}(y_{G_y})$ to perform x-direction reconstruction to get an approximation to $W(x_{i+\frac{1}{2}}, y_{G_y})$, i.e.,

$$\{\bar{W}_{mn}(y_{G_y}), \bar{W}_{x,mn}(y_{G_y})\} \to \tilde{W}(x_{i+\frac{1}{2}}, y_{G_y}) \approx W(x_{i+\frac{1}{2}}, y_{G_y}).$$

The reconstruction of $W(x_{G_x}, y_{j+\frac{1}{2}})$ is performed in a similar way.

3.3. The evaluation of the cell averages of W_x, W_y and W_{xy}

As in one dimensional case, the cell averages of W_x, W_y and W_{xy} need to be evaluated at the next time, which are given by

$$\begin{aligned}
\bar{V}_{ij}^{n+1} &= \frac{1}{\Delta x}\sum_{G_y} w_{G_y}(W(x_{i+\frac{1}{2}}, y_{G_y}, t_{n+1}) - W(x_{i-\frac{1}{2}}, y_{G_y}, t_{n+1})),\\
\bar{Y}_{ij}^{n+1} &= \frac{1}{\Delta y}\sum_{G_x} w_{G_x}(W(x_{G_x}, y_{j+\frac{1}{2}}, t_{n+1}) - W(x_{G_x}, y_{j-\frac{1}{2}}, t_{n+1})),\\
\bar{Z}_{ij}^{n+1} &= \frac{1}{\Delta x\Delta y}(W(x_{i+\frac{1}{2}}, y_{j+\frac{1}{2}}, t_{n+1}) - W(x_{i-\frac{1}{2}}, y_{j+\frac{1}{2}}, t_{n+1}) -\\
&\qquad (W(x_{i+\frac{1}{2}}, y_{j-\frac{1}{2}}, t_{n+1}) - W(x_{i-\frac{1}{2}}, y_{j-\frac{1}{2}}, t_{n+1}))).
\end{aligned} \tag{3.10}$$

Similar to one dimensional case, Li et al. [17] computed the values at next time using the non-equilibrium and equilibrium states. However, what is different from one dimensional case is that the computational costs are significantly increased in two dimensions since more terms at the next time should be evaluated for the numerical flux. Thus, the method developed in [17] becomes more complicated in two dimensions.

In this paper, to get $W(x_{i+\frac{1}{2}}, y_{G_y}, t_{n+1})$, τ is taken as Δt in (3.5) similar to the one dimensional case, which leads

$$W(x_{i+\frac{1}{2}}, y_{G_y}, t_n + \Delta t) = W(x_{i+\frac{1}{2}}, y_{G_y}, t_n^+) + \sum_{k=1}^{4}[\partial_t^{(k)} W(x_{j+\frac{1}{2}}, y_{G_y}, t_n^+)]\frac{(\Delta t)^k}{k!}. \tag{3.11}$$

$W(x_{G_x}, y_{j+\frac{1}{2}}, t_{n+1})$ and $W(x_{i+\frac{1}{2}}, y_{j+\frac{1}{2}}, t_{n+1})$ can be obtained in a similar way. Thus the values at the next time are evaluated by the Taylor expansion (3.11). The leading term and high order term also have been computed in the ADER method. Thus, we take trivial cost to obtain the value at different times and is simpler. In fact, we can employ the Gauss-Lobatto quadrature rule to evaluate the numerical flux. Thus, the values at the next time are calculated in the ADER method and can be directly used in (3.10) for updating the cell averages of the derivatives, which can further reduce the computational cost for our method.

4. The algorithm of the ADER-SHWENO method

Assume the physical solution is given at $t = t_n$. Now the procedure of the ADER-SHWENO method is summarized:

Algorithm 1 ADER-SHWENO method.

1: **Input:** $\left\{\bar{W}_j^n, \bar{V}_j^n\right\}$ at time level n
2: **Step I.** Reconstruct the pointwise values at the cell interface by (2.13).
3: **Step II.** Express all time derivatives as functions of space derivatives by (2.6).
4: **Step III.** Evaluate the values of the leading term and high order terms in (2.4) by (2.5) and (2.8), respectively.
5: **Step IV.** Compute the numerical flux (2.9).
6: **Step V.** Update the conservative variables by (2.2) and evaluate the cell average of derivatives at the next time by (2.14).
7: **Output:** $\left\{\bar{W}_j^{n+1}, \bar{V}_j^{n+1}\right\}$ at time level $n+1$

5. Numerical examples

In this section we present numerical results for a selection of one- and two-dimensional examples to demonstrate the performance of the ADER-SHWENO method proposed in the paper. The CFL condition number is taken as 0.9 for all the computations. In addition, the classic HWENO method [22] is termed as RK-HWENO in the following. In this paper, the two-dimensional RK-HWENO scheme is also reconstructed by a dimension-by-dimension strategy, and the procedure is the same as the two-dimensional SHWENO in Section 3.2. Moreover the CFL condition number for RK-HWENO is taken as 0.6. For accuracy test, we set time step $\Delta t = O(\Delta x^{\frac{5}{3}})$ for RK-HWENO method to make sure the spatial errors dominate. Moreover, the ADER scheme based on the simple WENO method [39] is termed as ADER-SWENO in the following.

5.1. One-dimensional examples

Example 5.1. We first consider Burgers' equation

$$W_t + \left(\frac{W^2}{2}\right)_x = 0, \quad x \in (0, 2)$$

Table 5.1
Example 5.1: Solution error with periodic boundary conditions and $t = \frac{0.5}{\pi}$.

method	N	10	20	40	80	160	320
ADER-SHWENO	L^1	7.320e-3	7.184e-4	1.729e-5	6.061e-7	1.977e-8	6.198e-10
	Order		3.349	5.377	4.834	4.938	4.995
	L^2	1.267e-2	1.324e-3	5.042e-5	1.738e-6	5.616e-8	1.768e-9
	Order		3.259	4.714	4.859	4.951	4.989
	L_∞	3.002e-2	4.208e-3	2.637e-4	9.512e-6	3.085e-7	9.941e-9
	Order		2.835	3.996	4.793	4.947	4.955
RK-HWENO	L^1	1.3887e-2	1.204e-3	6.052e-5	2.294e-6	8.357e-8	2.427e-9
	Order		3.525	4.315	4.722	4.779	5.106
	L^2	2.234e-2	2.808e-3	1.630e-4	5.974e-6	2.031e-7	6.086e-9
	Order		3.525	4.107	4.770	4.879	5.060
	L_∞	9.947e-2	1.079e-2	8.033e-4	3.290e-5	1.044e-6	3.175e-8
	Order		3.204	3.748	4.610	4.978	5.039
ADER-SWENO	L^1	1.701e-2	1.459e-3	6.180e-5	2.332e-6	7.602e-8	2.392e-9
	Order		3.543	4.561	4.728	4.939	4.990
	L^2	2.859e-2	2.958e-3	1.610e-4	6.338e-6	2.107e-7	6.687e-9
	Order		3.273	4.200	4.667	4.911	4.978
	L_∞	7.000e-2	1.039e-2	7.983e-4	3.369e-5	1.176e-6	3.773e-8
	Order		2.752	3.703	4.566	4.841	4.961

subject to the initial condition $W(x,0) = 0.5 + \sin(\pi x)$ and a periodic boundary condition.

We compute the solution up to $t = \frac{0.5}{\pi}$ when the solution is still smooth and the exact solution can be computed using Newton's iteration. The errors of the ADER-SHWENO, RK-HWENO and ADER-SWENO method are listed in Table 5.1, which shows the convergence of the fifth order for all the methods. Moreover, from the table one can observe that the error of the ADER-SHWENO method is smallest among the three methods at the same number of points.

Example 5.2. To see the accuracy of the method for system problems, we compute the Euler equations,

$$\begin{pmatrix} \rho \\ \rho u \\ E \end{pmatrix}_t + \begin{pmatrix} \rho u \\ \rho u^2 + P \\ u(E+P) \end{pmatrix}_x = 0, \tag{5.1}$$

where ρ is the density, u is the velocity, E is the energy density, and P is the pressure. The equation of state is $E = \frac{P}{\gamma - 1} + \frac{1}{2}\rho u^2$ with $\gamma = 1.4$. The initial condition is

$$\rho(x,0) = 1 + 0.2\sin(\pi x), \quad u(x,0) = 1, \quad P(x,0) = 1,$$

and a periodic boundary condition is used. The exact solution for this problem is

$$\rho(x,t) = 1 + 0.2\sin(\pi(x-t)), \quad u(x,t) = 1, \quad P(x,t) = 1.$$

The final time is $t = 10.0$. The errors of both ADER-SHWENO, RK-HWENO and ADER-SWENO method in computed density are listed in Table 5.2. From the table one can see that the fifth order of accuracy of the scheme is achieved for this nonlinear system for all the methods. Moreover the error of ADER-SHWENO method is also smallest among all the methods, which is the same as the Example 5.1. In addition, the accuracy will be decreased to third order for RK-HWENO if the time step is set as $\Delta t = O(\Delta x)$.

To show the efficiency of the ADER-SHWENO method, we plot the L^∞ error as a function of the CPU time for both RK-HWENO and ADER-SHWENO methods in Fig. 5.1. The results are obtained on a single Intel Core i7 CPU with 2.5 GHz and 32.00 GB of RAM using Matlab R2021b. From the figure, one can see that the ADER-SHWENO method is more efficient than the original RK-HWENO method.

Example 5.3. In this example we consider the Lax problem of the Euler equations (5.1) with the initial condition

$$(\rho, u, p) = \begin{cases} (0.445, 0.698, 3.528), & \text{for} \quad x < 0 \\ (0.5, 0, 0.571), & \text{for} \quad x > 0 \end{cases}$$

and the inflow/outflow boundary condition. The computational domain is $(-5, 5)$ and the integration is stopped at $t = 1.3$.

The computed density obtained by the RK-HWENO and ADER-SHWENO methods is plotted with 200 points in Fig. 5.2, in which one can see that the resolution obtained by ADER-SHWENO is comparable with that obtained by RK-HWENO.

Example 5.4. The Shu-Osher problem is considered in this example, which contains both shocks and complex smooth region structures. We solve the Euler equations (5.1) with a moving shock (Mach = 3) interacting with a sine wave in density. The initial condition is

Table 5.2
Example 5.2: Errors in computed density for periodic boundary conditions and $t = 10.0$.

method	N	10	20	40	80	160
ADER-SHWENO	L^1	1.328e-3	4.031e-5	1.274e-6	3.983e-8	1.244e-9
	Order		5.043	4.984	4.999	5.001
	L^2	1.556e-3	4.545e-5	1.417e-6	4.423e-8	1.382e-9
	Order		5.097	5.003	5.002	5.001
	L_∞	2.263e-3	6.976e-5	2.032e-6	6.271e-8	1.954e-9
	Order		5.020	5.102	5.018	5.004
RK-HWENO	L^1	1.276e-2	5.794e-4	1.730e-5	5.346e-7	1.648e-8
	Order		4.461	5.066	5.016	5.020
	L^2	1.375e-2	6.335e-4	1.974e-5	6.041e-7	1.862e-8
	Order		4.440	5.002	5.033	5.020
	L_∞	1.660e-2	9.258e-4	3.218e-5	1.010e-6	3.008e-8
	Order		4.164	4.846	4.994	5.069
ADER-SWENO	L^1	6.422e-3	1.478e-4	4.819e-6	1.519e-7	4.718e-9
	Order		5.441	4.939	4.996	5.000
	L^2	7.546e-3	1.734e-4	5.362e-6	1.677e-7	5.240e-9
	Order		5.444	5.015	4.999	5.000
	L_∞	1.123e-3	3.008e-4	7.882e-6	2.394e-7	7.419e-9
	Order		5.222	5.254	5.041	5.012

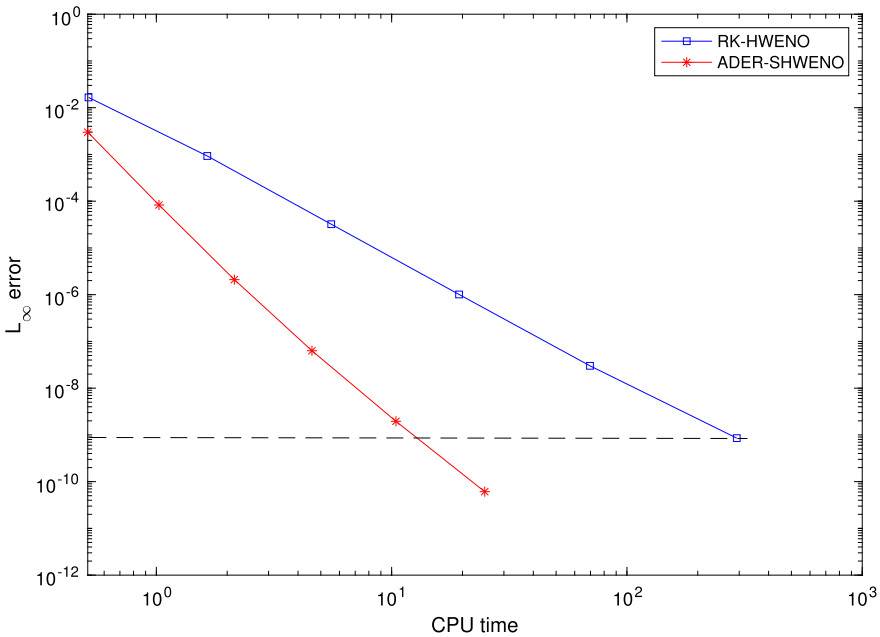

Fig. 5.1. L_∞ error is plotted as a function of CPU time (in seconds).

$$(\rho, u, p) = \begin{cases} (3.857143, 2.629369, 10.333333), & \text{for} \quad x < -4, \\ (1 + 0.2\sin(5x), 0, 1), & \text{for} \quad x > -4. \end{cases}$$

The physical domain is taken as $(-5, 5)$ in this computation. The computed density is shown at $t = 1.8$ against an "exact solution" obtained by a fifth-order finite volume WENO scheme with 10,000 uniform points.

The solution obtained by the ADER-SHWENO method with 400 uniform points is compared with the uniform mesh solutions obtained by the RK-HWENO method and ADER-SWENO method in Fig. 5.3 and 5.4, respectively. From the figures, one can observe that the results obtained by ADER-SHWENO method are better than ones obtained by RK-HWENO method, and comparable with ones obtained by the ADER-SWENO method. However, ADER-SHWENO method is more compact than ADER-SWENO method.

Example 5.5. In this example the turbulence interaction [32] is considered. The computational domain is taken as $(-5, 5)$. The initial condition is given by

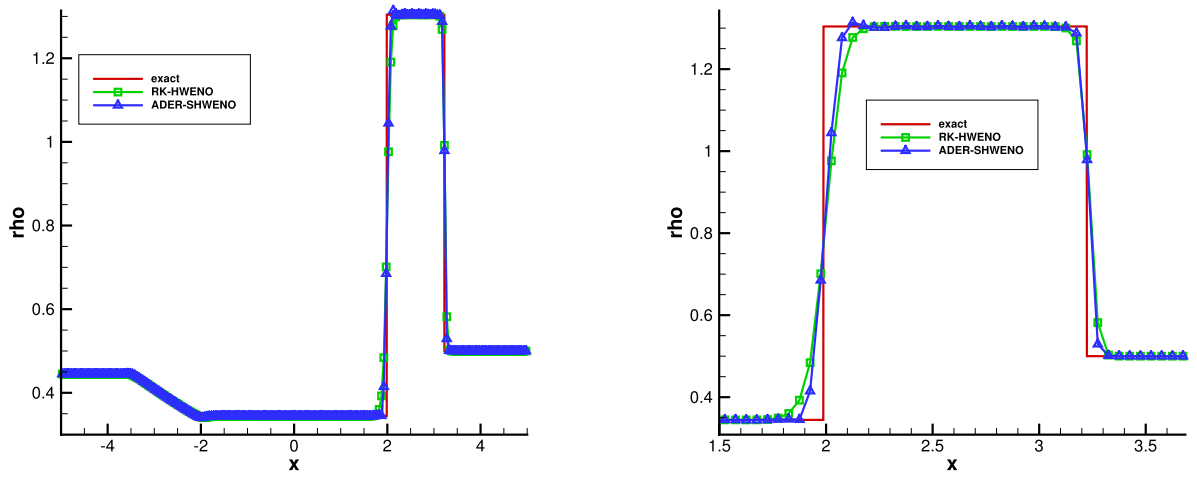

Fig. 5.2. Example 5.3: The density obtained by ADER-SHWENO method with $N = 200$ uniform meshes is compared with RK-HWENO method. Green square: RK-HWENO; Blue triangle: ADER-SHWENO. (For interpretation of the colors in the figure(s), the reader is referred to the web version of this article.)

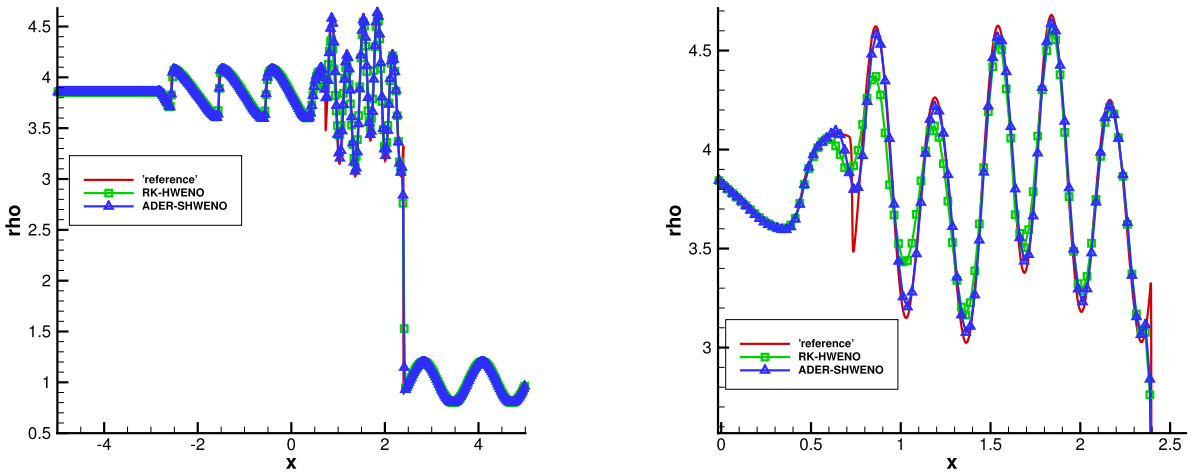

Fig. 5.3. Example 5.4: The density obtained by ADER-SHWENO method with $N = 400$ uniform meshes is compared with RK-HWENO method. Green square: RK-HWENO; Blue triangle: ADER-SHWENO.

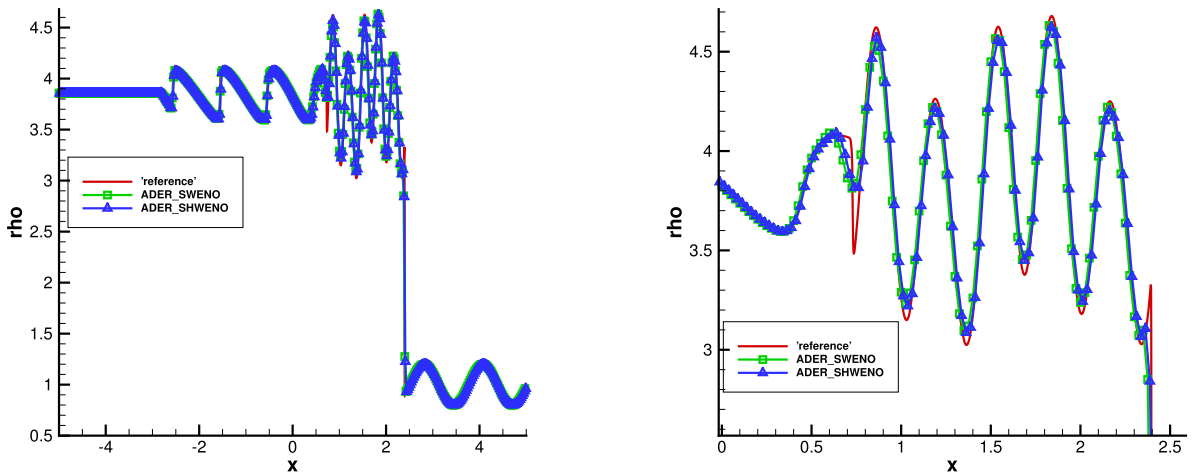

Fig. 5.4. Example 5.4: The density obtained by ADER-SHWENO method with $N = 400$ uniform meshes is compared with ADER-SWENO method. Green square: ADER-SWENO; Blue triangle: ADER-SHWENO.

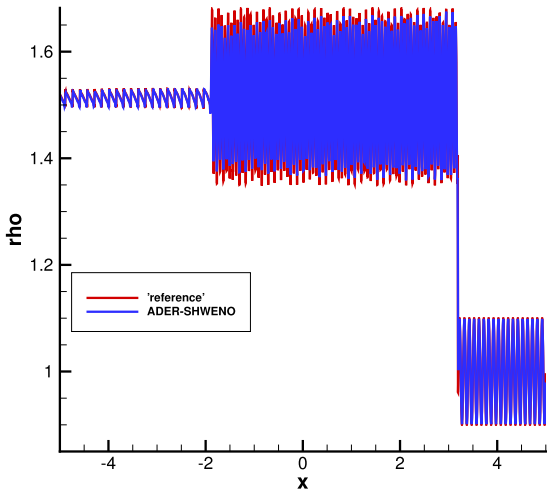

(a) ADER-SHWENO

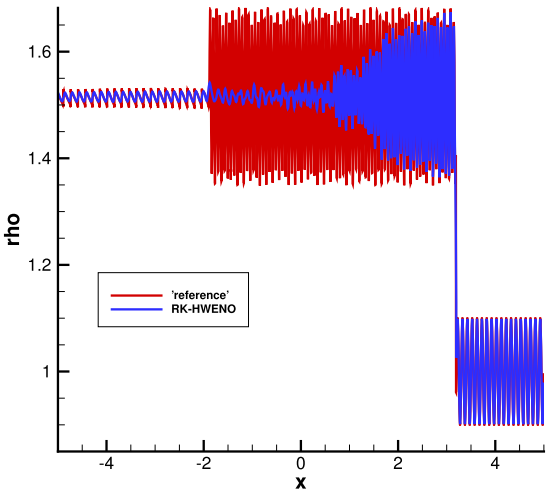

(b) RK-HWENO

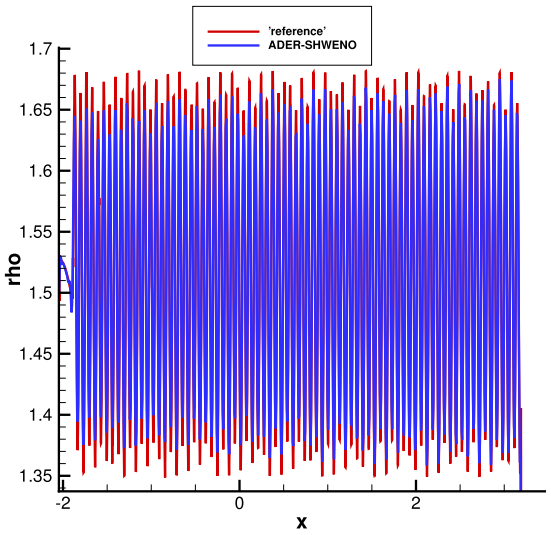

(c) zoom of (a)

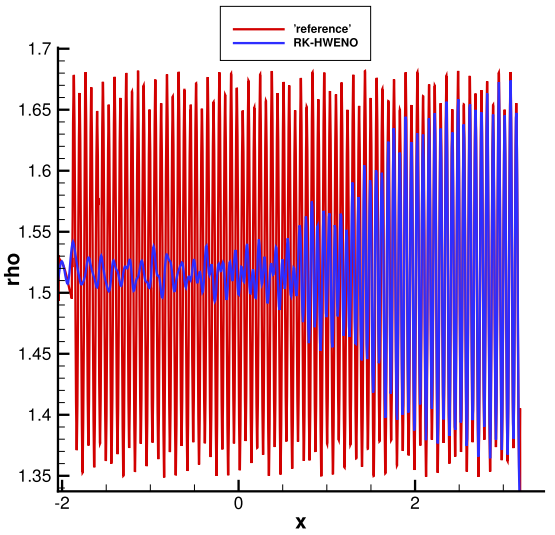

(d) zoom of (b)

Fig. 5.5. The density obtained by ADER-SHWENO method with $N = 1500$ uniform meshes is compared with RK-HWENO method.

$$(\rho, u, p) = \begin{cases} (1.515695, 0.523346, 1.80500), & \text{for} \quad x < -4.5 \\ (1 + 0.1\sin(20\pi x), 0, 1), & \text{for} \quad x > -4.5. \end{cases}$$

The results of the computed density obtained by both methods with 1500 uniform meshes are plotted at $t = 5$ against a "reference solution" obtained by the ADER-SHWENO method with 10,000 uniform points.

From Fig. 5.5, one can see that the resolution of the ADER-SHWENO method is much better than that of the RK-HWENO method, which shows the advantages of the new method for the problem containing the complex structure.

Example 5.6. We consider the interaction of blast waves of the Euler equations (5.1), which was first used by Woodward and Colella [35] as a test problem for various numerical schemes. The initial condition is given by

$$(\rho, u, p) = \begin{cases} (1.0, 0, 1000), & \text{for} \quad 0 \le x < 0.1 \\ (1.0, 0, 0.01), & \text{for} \quad 0.1 \le x < 0.9 \\ (1.0, 0, 100), & \text{for} \quad 0.9 \le x \le 1. \end{cases}$$

The physical domain is taken as $(0, 1)$ and a reflective boundary condition is applied to both ends. The results at time $t = 0.038$ are plotted against an "exact solution" computed by a fifth-order finite difference WENO scheme [12] with 81,920 uniform mesh points in Fig. 5.6 and Fig. 5.7.

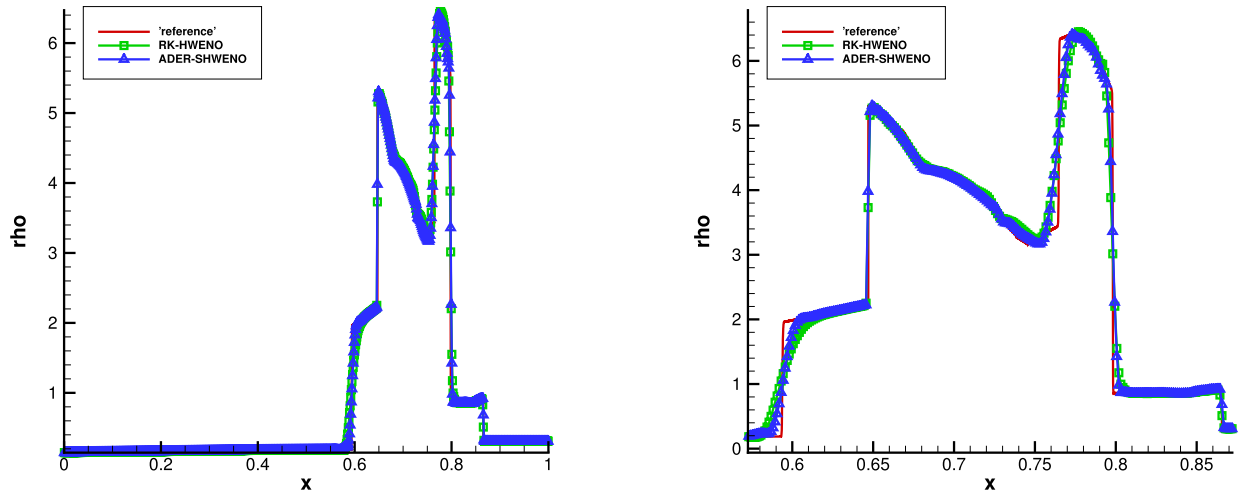

Fig. 5.6. Example 5.6: The density obtained by ADER-SHWENO method with $N = 800$ uniform meshes is compared with RK-HWENO method. Green square: RK-HWENO; Blue triangle: ADER-SHWENO.

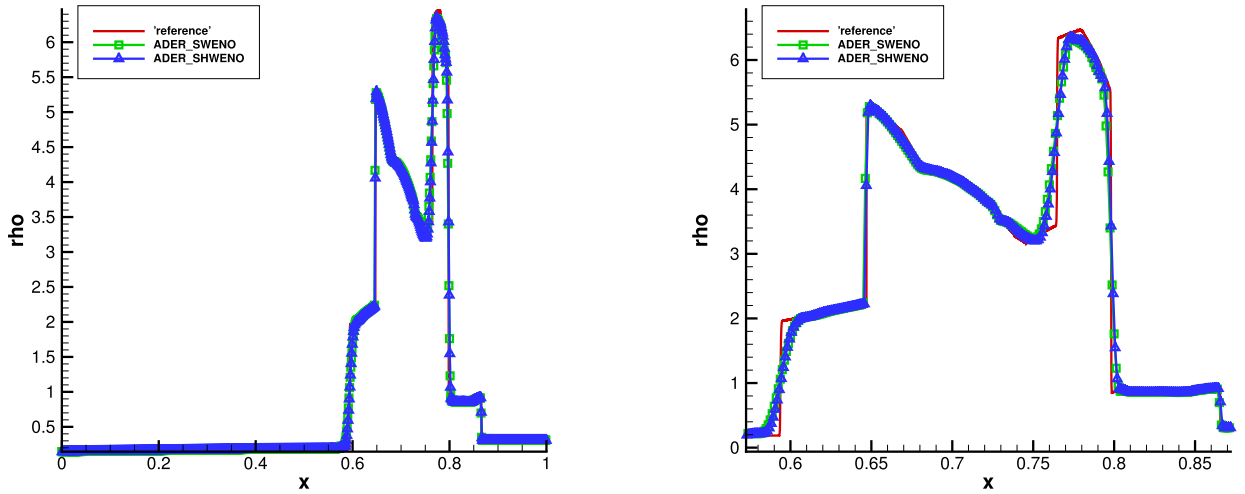

Fig. 5.7. Example 5.6: The density obtained by ADER-SHWENO method with $N = 800$ uniform meshes is compared with ADER-SWENO method. Green square: ADER-SWENO; Blue triangle: ADER-SHWENO.

From the figures we can see that the solution obtained by ADER-SHWENO method is comparable with that obtained by RK-HWENO method and ADER-SWENO method.

5.2. Two-dimensional examples

Example 5.7. In order to test the accuracy in two-dimensional case, we solve the Euler equations

$$W_t + F(W)_x + G(W)_y \equiv \frac{\partial}{\partial t}\begin{pmatrix}\rho\\ \rho\mu\\ \rho\nu\\ E\end{pmatrix} + \frac{\partial}{\partial x}\begin{pmatrix}\rho\mu\\ \rho\mu^2+P\\ \rho\mu\nu\\ \mu(E+P)\end{pmatrix} + \frac{\partial}{\partial y}\begin{pmatrix}\rho\nu\\ \rho\mu\nu\\ \rho\nu^2+P\\ \nu(E+P)\end{pmatrix} = 0, \tag{5.2}$$

where ρ is the density, μ and ν are the velocity components in the x- and y-direction, respectively, E is the energy density, and P is the pressure. The equation of state is $E = \frac{P}{\gamma-1} + \frac{1}{2}\rho(\mu^2+\nu^2)$ with $\gamma = 1.4$. The initial condition is given by

$$\rho(x,y,0) = 1 + 0.2\sin(\pi(x+y)),\ \mu(x,y,0) = 1,\ \nu(x,y,0) = 1,\ P(x,y,0) = 1,$$

and a periodic boundary condition is applied in both directions.

Table 5.3
Example 5.7: Solution error with periodic boundary conditions and $t = 1$.

method	$N \times M$	10×10	20×20	40×40	80×80	160×160
ADER-SHWENO	L^1	8.405e-4	8.659e-6	2.584e-7	7.873e-9	2.427e-10
	Order		6.601	5.067	5.037	5.020
	L^2	1.101e-3	9.391e-6	2.833e-7	8.692e-9	2.689e-10
	Order		6.873	5.051	5.026	5.015
	L_∞	1.887e-3	1.558e-5	4.080e-7	1.232e-8	3.820e-10
	Order		6.920	5.255	5.049	5.011
RK-HWENO	L^1	9.860e-3	3.836e-4	1.106e-5	3.344e-7	1.024e-8
	Order		4.684	5.116	5.048	5.029
	L^2	1.036e-2	4.078e-4	1.231e-5	3.735e-7	1.143e-8
	Order		4.667	5.050	5.043	5.030
	L_∞	1.340e-2	5.734e-4	1.983e-5	6.213e-7	1.820e-8
	Order		4.547	4.854	4.996	5.093

Table 5.4
Example 5.8: Solution error with periodic boundary conditions and $t = 10$.

method	$N \times M$	10×10	20×20	40×40	80×80	160×160	320×320
ADER-SHWENO	L^1	1.870e-2	2.834e-3	1.113e-4	4.073e-6	1.329e-7	4.693e-9
	Order		2.722	4.670	4.771	4.938	4.824
	L^2	4.286e-2	5.972e-3	2.879e-4	1.160e-5	3.835e-7	1.219e-8
	Order		2.843	4.375	4.633	4.919	4.976
	L_∞	3.447e-1	5.292e-2	1.883e-3	7.588e-5	2.506e-6	7.822e-8
	Order		2.703	4.813	4.633	4.920	5.002
RK-HWENO	L^1	2.609e-2	1.442e-2	7.669e-3	4.481e-3	2.074e-4	1.123e-6
	Order		0.855	0.911	0.775	4.433	7.529
	L^2	5.638e-2	3.372e-2	1.666e-2	1.057e-2	4.901e-4	1.719e-6
	Order		0.742	1.017	0.656	4.431	8.155
	L_∞	4.389e-1	2.506e-1	1.348e-1	8.709e-2	8.295e-3	1.171e-5
	Order		0.809	0.895	0.630	3.392	9.468

The computational domain is $(0, 2) \times (0, 2)$ and the final time is $t = 1$. The results in Table 5.3 show the convergence of the fifth order for both ADER-SHWENO and RK-HWENO method is achieved for the Euler system in two dimensions. In addition, the error of ADER-SHWENO is much smaller than that of RK-HWENO.

Example 5.8. In this example, the two-dimensional isotropic vortex problem is considered. The computational domain is taken as $(0, 10) \times (0, 10)$ and the initial condition is

$$\rho = (1 - \frac{25(\gamma-1)}{8\gamma\pi^2} e^{1-r^2})^{\frac{1}{\gamma-1}}, \mu = 1 - \frac{5}{2\pi} e^{\frac{1-r^2}{2}} (y-5), \nu = 1 + \frac{5}{2\pi} e^{\frac{1-r^2}{2}} (x-5), P = \rho^\gamma,$$

where $r^2 = (x-5)^2 + (y-5)^2$. The periodic boundary condition is employed in both directions. The exact solution is the vortex along the upper right direction with velocities $(\mu, \nu) = (1, 1)$. We compute the numerical solution at the output time $t = 10$. At this time the vortex returns to the initial position.

The errors of the computed density are listed in Table 5.4 for both methods, in which one can observe that both ADER-SHWENO method can achieve the fifth order accuracy for this nonlinear smooth problem. From the table one can see that the error of ADER-SHWENO is much smaller the same as the previous example.

Example 5.9. To show the performance of our method for Riemann problem genuinely in two dimensions, two 2D Riemann problems are considered in the example. The first one we consider is a 2D Riemann problem with shock waves [13] with the initial condition

$$(\rho, \mu, \nu, P) = \begin{cases} (1.1, 0.0, 0.0, 1.1), & \text{if } x > 0.5,\ y > 0.5, \\ (0.5065, 0.8939, 0.0, 0.35), & \text{if } x < 0.5,\ y > 0.5, \\ (1.1, 0.8939, 0.8939, 1.1), & \text{if } x < 0.5,\ y < 0.5, \\ (0.5065, 0.0, 0.8939, 0.35), & \text{if } x > 0.5,\ y < 0.5, \end{cases}$$

which is the case of left forward shock, right backward shock, upper backward shock and lower forward shock in [13]. And the non-reflecting boundary conditions are employed on all the boundaries. The computational domain is taken as $(0, 1) \times (0, 1)$ and the stop time is taken as 0.25.

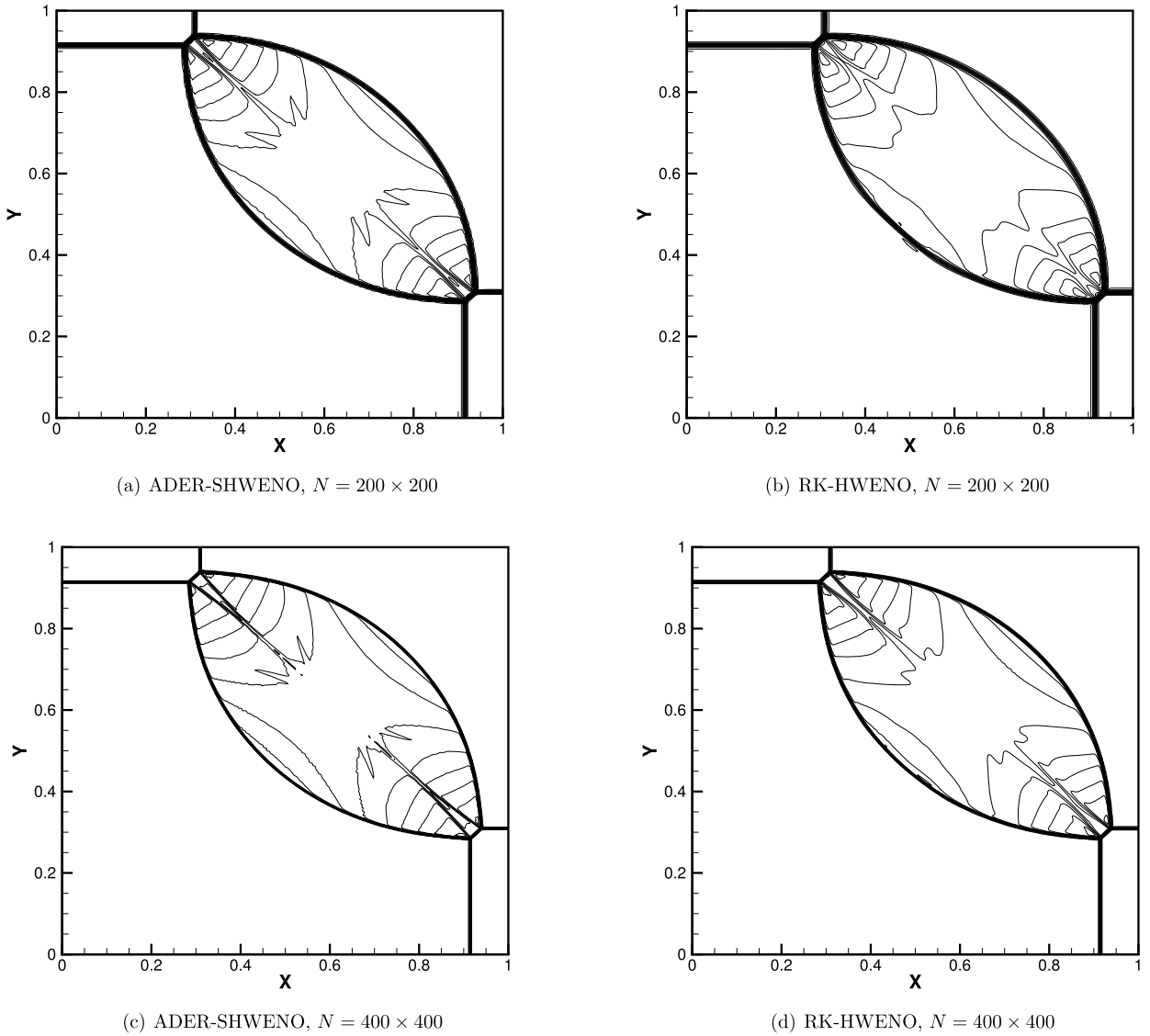

(a) ADER-SHWENO, $N = 200 \times 200$

(b) RK-HWENO, $N = 200 \times 200$

(c) ADER-SHWENO, $N = 400 \times 400$

(d) RK-HWENO, $N = 400 \times 400$

Fig. 5.8. Example 5.9: 30 density contours from 0.5 to 1.9.

The computed density contours using both methods with 200×200 and 400×400 uniform meshes are plotted in Fig. 5.8, which shows that the results obtained by the refiner mesh have a better resolution. Besides, one can observe that the results are comparable for both methods from the figures.

The second problem is the shear instabilities among four initial contact discontinuities [13,17]. The initial condition is given by

$$(\rho, \mu, v, P) = \begin{cases} (1.0, 0.75, -0.5, 1.0), & \text{if } x > 0.5,\ y > 0.5, \\ (2.0, 0.5, 0.5, 1.0), & \text{if } x < 0.5,\ y > 0.5, \\ (1.0, -0.75, 0.5, 1.0), & \text{if } x < 0.5,\ y < 0.5, \\ (3.0, -0.75, -0.5, 1.0), & \text{if } x > 0.5,\ y < 0.5. \end{cases}$$

And the non-reflecting boundary conditions are adopted on all the boundaries. The computational domain is taken as $(0, 1) \times (0, 1)$.

Fig. 5.9 is the result of the density computed by the ADER-SHWENO and RK-HWENO methods with 200×200 and 400×400 uniform meshes at $t = 0.8$. From the figure, one can observe that more complex structures are captured for the refiner mesh. Moreover, the ADER–SHWENO method captures more complex structures than the RK-HWENO method, which indicates the advantages of the newly-developed method.

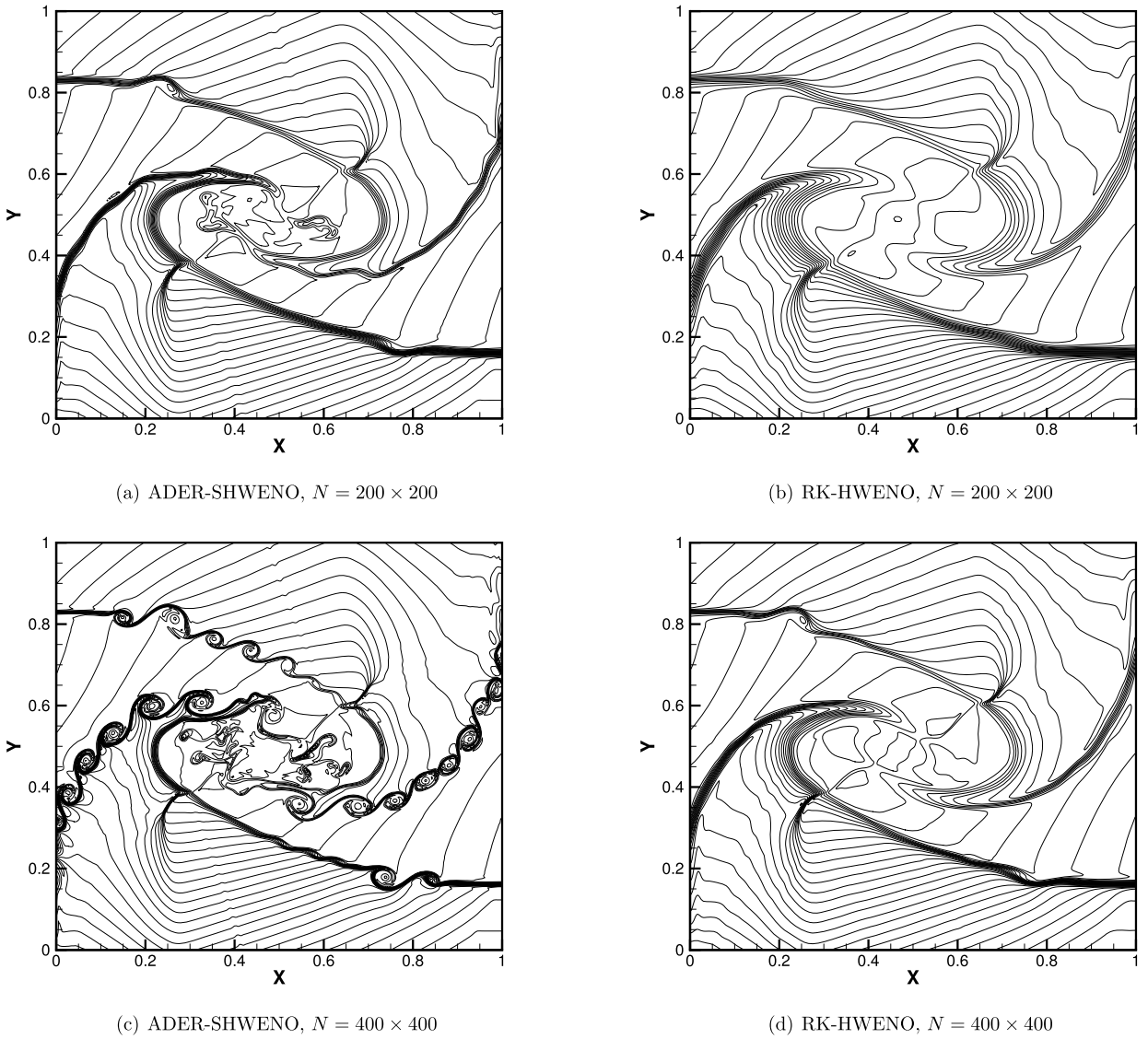

(a) ADER-SHWENO, $N = 200 \times 200$

(b) RK-HWENO, $N = 200 \times 200$

(c) ADER-SHWENO, $N = 400 \times 400$

(d) RK-HWENO, $N = 400 \times 400$

Fig. 5.9. Example 5.9: 30 density contours from 0.2 to 2.4.

Example 5.10. This is the double Mach reflection problem [35]. We solve the Euler equations (5.2) in a computational domain of $(0,4) \times (0,1)$. The initial condition is given by

$$W = \begin{cases} (8, 57.1597, -33.0012, 563.544)^T, & \text{for} \quad y \geq h(x,0) \\ (1.4, 0, 0, 2.5)^T, & \text{otherwise} \end{cases}$$

where $h(x,t) = \sqrt{3}(x - \frac{1}{6}) - 20t$. The exact post shock condition is imposed from 0 to $\frac{1}{6}$ at the bottom while the reflection boundary condition for the rest of the bottom boundary. At the top, the boundary condition is the values that describe the exact motion of the Mach 10 shock. On the left and right boundaries, the inflow and outflow boundary conditions are used, respectively. The final time is $t = 0.2$.

The density contours are shown in Fig. 5.10 on $(0,3) \times (0,1)$. The complex regions are plotted in Fig. 5.11. From the figures, one can see that the resolution is improved as the meshes are refined. In addition, more complex vortex are captured by the ADER-SHWENO method.

6. Conclusions

We have presented a compact and high order ADER scheme using the simple HWENO method for hyperbolic conservation laws. The Lax-Wendroff procedure is adopted in the newly-developed method to convert time derivatives to spatial derivatives, which

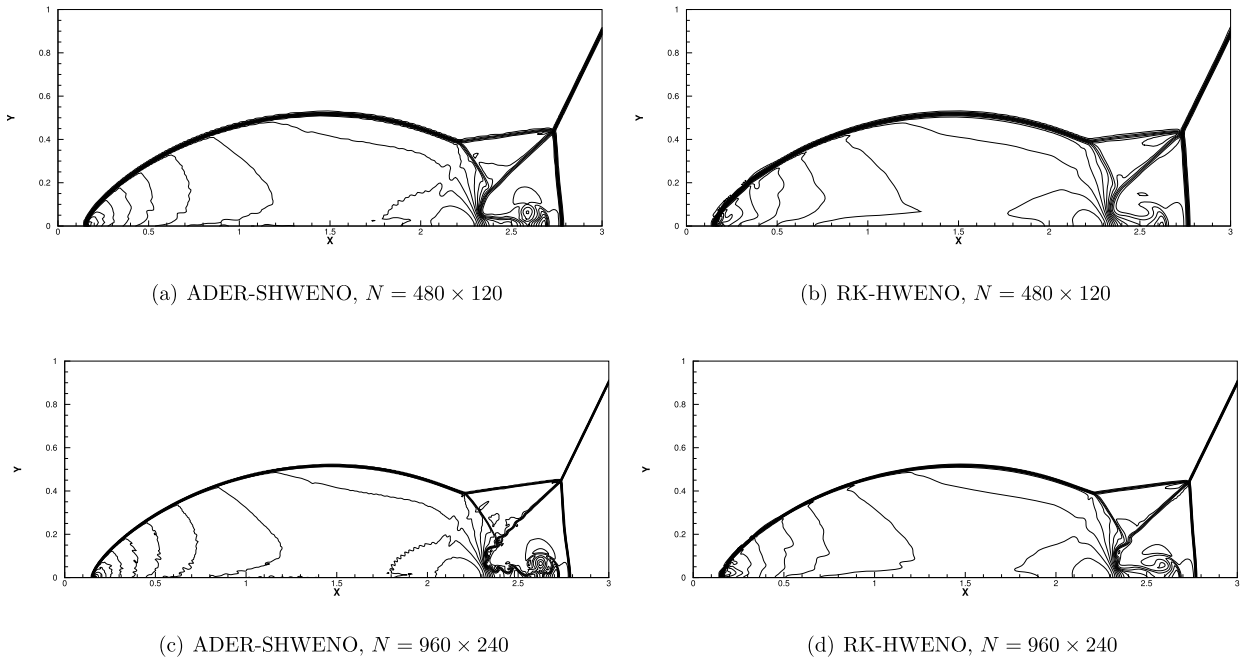

(a) ADER-SHWENO, $N = 480 \times 120$

(b) RK-HWENO, $N = 480 \times 120$

(c) ADER-SHWENO, $N = 960 \times 240$

(d) RK-HWENO, $N = 960 \times 240$

Fig. 5.10. Example 5.10: 30 density contours from 2 to 22.

provides the time evolution of the variables at the cell interface. This information is necessary for the SHWENO reconstructions, which take advantages of the simple WENO [38,39] and the classic HWENO [22,23]. Compared with the original RK-HWENO [22,23], the new method has two advantages. Firstly, RK-HWENO method must solve the additional equations for reconstructions, which is avoided for the new method. Secondly, the SHWENO reconstruction is performed once with one stencil and is different from the classic HWENO methods, in which both the function and its derivative values are reconstructed with two different stencils, respectively. Thus the new method is more efficient than the RK-HWENO method. Moreover, the new method makes the best use of the information in the ADER method. Therefore the time evolutions of the cell averages of the derivatives are simpler than that developed in the work [17], where it includes the non-equilibrium and equilibrium parts. Besides, the new method is more compact than the ADER-WENO [28]. Numerical results in one and two dimensions shown demonstrate the high order for smooth solutions both in space and time and keep non-oscillatory at discontinuities. We recall that the structured mesh has been used in this work. Extending the developed method to the unstructured mesh has been underway. In addition, we will combine the ADER-SHWENO with the moving mesh method [19] to further improve the resolution.

CRediT authorship contribution statement

Dongmi Luo: Conceptualization, Methodology, Software, Writing – original draft. **Shiyi Li:** Methodology. **Jianxian Qiu:** Methodology, Writing – review & editing. **Jun Zhu:** Methodology. **Yibing Chen:** Conceptualization, Methodology, Supervision, Writing – review & editing.

Declaration of competing interest

The authors declare that they have no known competing financial interests or personal relationships that could have appeared to influence the work reported in this paper.

Data availability

The data that has been used is confidential.

Acknowledgements

D. M. Luo gratefully thanks Dr. Chuan Fan at Southern University of Science and Technology for providing the numerical solutions of Navier-Stokes equations as a comparison.

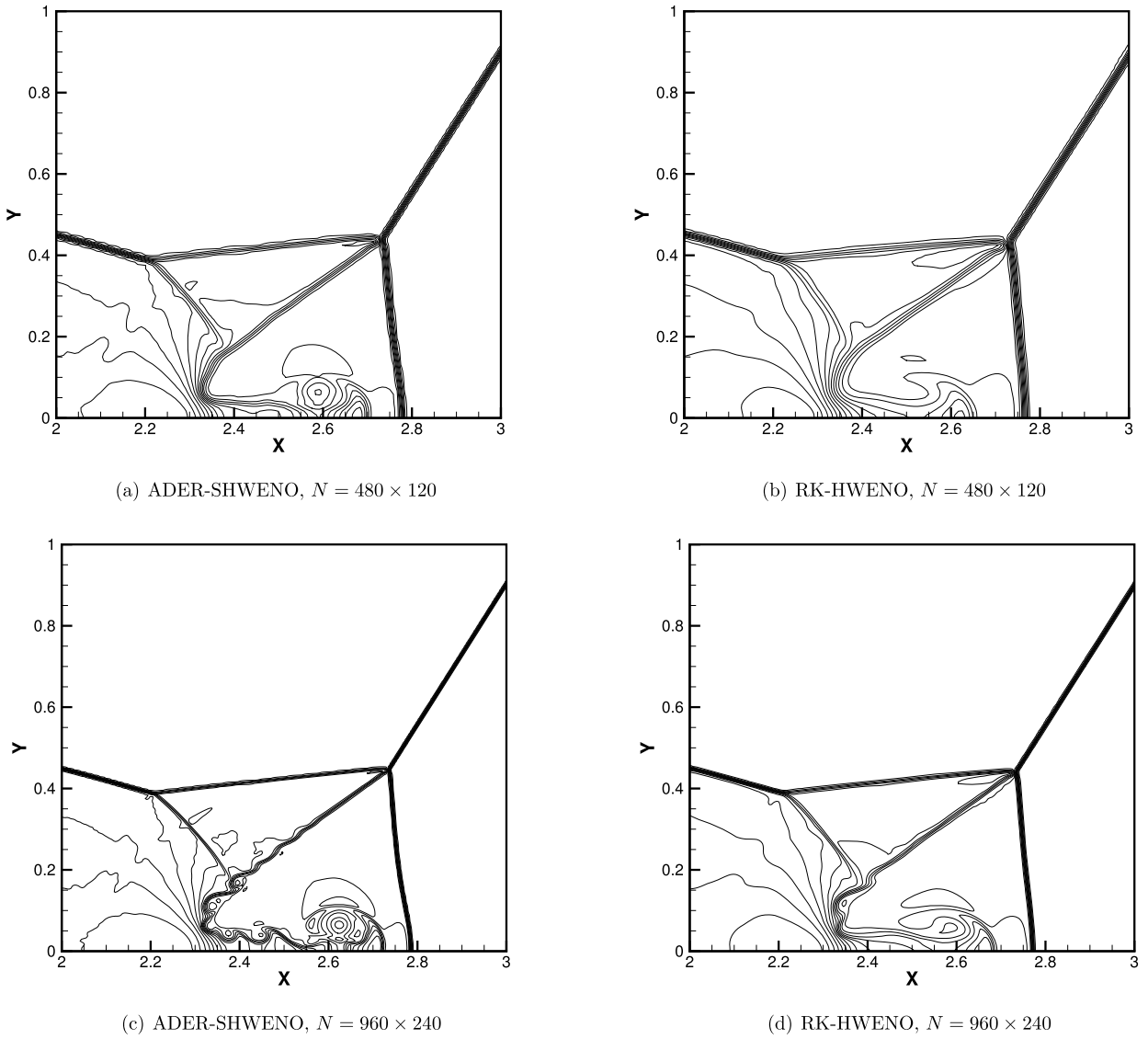

(a) ADER-SHWENO, $N = 480 \times 120$

(b) RK-HWENO, $N = 480 \times 120$

(c) ADER-SHWENO, $N = 960 \times 240$

(d) RK-HWENO, $N = 960 \times 240$

Fig. 5.11. Example 5.10: 30 density contours from 2 to 22. Zoom of Fig. 5.10 in the complex region.

Appendix A

In this paper, the Euler equations are focused on. However the ADER-SHWENO method can be also extended to the viscous Navier-Stokes equations with the same idea as the previous section described. For simplicity the ADER-SHWENO method for the viscous Navier-Stokes equations in one dimension is given briefly in the following and the two-dimensional can be implemented similarly, which have the form of [4,34]:

$$\begin{cases} W_t + F(W)_x = G(W, W_x)_x, \\ W(x,0) = W_0(x), \end{cases} \tag{6.1}$$

where the conservative variables W and the flux function $F(W)$ are the same as (5.1), and

$$G(W, W_x) = \begin{pmatrix} 0 \\ \frac{4}{3}\mu u_x \\ \frac{4}{3}\mu u u_x + \frac{\mu}{P_r(\gamma-1)} T_x \end{pmatrix}, \tag{6.2}$$

where T is the temperature, P_r is the Prandtl number and μ is the molecular viscosity computed by the Sutherland's law

$$\mu = \frac{1+c}{T+c} T^{\frac{3}{2}},$$

where $c = \frac{110.4}{T_\infty}$, and $T_\infty = 288K$ is the reference temperature. The temperature is related to the pressure and density as

$$T = \frac{P}{\rho R},$$

where R is the gas constant. For simplicity, the gas constant R is set to be 1 and μ is taken as a constant in this paper.

Then the finite volume method for the equation (6.1) is defined

$$\bar{W}_j^{n+1} = \bar{W}_j^n - \frac{\Delta t}{\Delta x}(\hat{F}_{j+\frac{1}{2}} - \hat{F}_{j-\frac{1}{2}}) + \frac{\Delta t}{\Delta x}(\hat{G}_{j+\frac{1}{2}} - \hat{G}_{j-\frac{1}{2}}), \tag{6.3}$$

where $\hat{G}_{j+\frac{1}{2}} \approx \frac{1}{\Delta t}\int_{t_n}^{t_{n+1}} G(W, W_x)_{j+\frac{1}{2}} dt$ is the numerical flux for the diffusion term. To evaluate the numerical flux an appropriate Gaussian rule is used similarly to (2.9)

$$\hat{F}_{j+\frac{1}{2}} = \sum_{\alpha=0}^{K_\alpha} \tilde{F}(W(x_{j+\frac{1}{2}}, \lambda_\alpha \Delta t))w_\alpha, \tag{6.4}$$

$$\hat{G}_{j+\frac{1}{2}} = \sum_{\alpha=0}^{K_\alpha} \tilde{G}(W(x_{j+\frac{1}{2}}, \lambda_\alpha \Delta t), W_x(x_{j+\frac{1}{2}}, \lambda_\alpha \Delta t))w_\alpha, \tag{6.5}$$

where λ_α and w_α are properly scaled nodes and weights of the rule, and K_α is the number of the nodes.

Recall that the leading term of the Taylor series expansion (2.4) is the solution of a nonlinear problem obtained by an exact or approximate non-linear Riemann solver and the high order terms are obtained by solving linearized Riemann problem, which are adopted for the evaluation of the flux (2.9). However for complex nonlinear systems such solvers are very complicated. Besides, in the appendix our main goal is to show the ADER-SHWENO method can be extended to the Navier-Stokes equations. Thus the simple Lax-Friedrichs flux and the central flux are employed for the advection term (6.4) and the diffusion term (6.5), respectively, i.e.,

$$\tilde{F}_{j+\frac{1}{2}} = \frac{1}{2}(F(W(x^-_{j+\frac{1}{2}}, \tau) + F(W(x^+_{j+\frac{1}{2}}, \tau)) - \alpha(W(x^+_{j+\frac{1}{2}}, \tau) - W(x^-_{j+\frac{1}{2}}, \tau))),$$

$$\tilde{G}_{j+\frac{1}{2}} = \frac{1}{2}(G(W(x^-_{j+\frac{1}{2}}, \tau), W_x(x^-_{j+\frac{1}{2}}, \tau)) + G(W(x^+_{j+\frac{1}{2}}, \tau), W_x(x^+_{j+\frac{1}{2}}, \tau))),$$

where $\tau = \lambda_\alpha \Delta t$, and α is the numerical viscosity constant taken as the largest eigenvalues in magnitude of $\max_j |F'(\bar{W}_j, \tau)|$. Then the approximate solutions at time $t = \tau$ on each side of the interface $x_{j+\frac{1}{2}}$ are evaluated by

$$W(x^-_{j+\frac{1}{2}}, \tau) \approx W(x^-_{j+\frac{1}{2}}, 0^+) + \sum_{k=1}^{4} [\partial_t^{(k)} W(x^-_{j+\frac{1}{2}}, 0^+)] \frac{\tau^k}{k!}, \tag{6.6}$$

$$W(x^+_{j+\frac{1}{2}}, \tau) \approx W(x^+_{j+\frac{1}{2}}, 0^+) + \sum_{k=1}^{4} [\partial_t^{(k)} W(x^+_{j+\frac{1}{2}}, 0^+)] \frac{\tau^k}{k!}. \tag{6.7}$$

Similarly, the values of $W_x(x^+_{j+\frac{1}{2}}, \tau)$ used for diffusion flux are obtained

$$W_x(x^-_{j+\frac{1}{2}}, \tau) \approx W_x(x^-_{j+\frac{1}{2}}, 0^+) + \sum_{k=1}^{3} [\partial_t^{(k)} W_x(x^-_{j+\frac{1}{2}}, 0^+)] \frac{\tau^k}{k!}, \tag{6.8}$$

$$W_x(x^+_{j+\frac{1}{2}}, \tau) \approx W_x(x^+_{j+\frac{1}{2}}, 0^+) + \sum_{k=1}^{3} [\partial_t^{(k)} W_x(x^+_{j+\frac{1}{2}}, 0^+)] \frac{\tau^k}{k!}. \tag{6.9}$$

From the last two equations above, one can observe that the order of the method will be decreased to four for the advection-diffusion equations. Moreover, all time derivatives are also expressed as functions of space derivatives by the Lax-Wendroff procedure based on the equation (6.1) at present. And the equation (6.1) is written as

$$W_t + F(W)_x = G(W, W_x)_x = (D(W)W_x)_x \tag{6.10}$$

where $D(W) = \frac{\partial G(W, W_x)}{\partial W_x}$ is a matrix. Thus similar to (2.6), one can get the following expressions:

$$\partial_t W = -\frac{\partial F}{\partial W}\partial_x W + (\frac{\partial D}{\partial W}\partial_x W)\partial_x W + D\partial_{xx} W,$$

$$\partial_{tx} W = -(\frac{\partial^2 F}{\partial W^2}\partial_x W)\partial_x W - \frac{\partial F}{\partial W}\partial_{xx} W + (\frac{\partial^2 D}{\partial W^2}\partial_x W)\partial_x W \partial_x W + (\frac{\partial D}{\partial W}\partial_{xx} W)\partial_x W + (\frac{\partial D}{\partial W}\partial_x W)\partial_{xx} W + (\frac{\partial D}{\partial W}\partial_x W)\partial_{xx} W + D\partial_{xxx} W,$$

Table 6.1
Example 6.1: Solution errors with periodic boundary conditions, $t = 1.0$ and $\epsilon = 0.01$.

method	N	10	20	40	80	160	320
ADER-SHWENO	L^1	2.826e-3	1.713e-4	3.825e-7	9.392e-9	2.984e-10	9.490e-12
	Order		4.045	8.807	5.348	4.976	4.975
	L^2	3.990e-3	2.632e-4	4.449e-7	1.051e-8	3.316e-10	1.054e-11
	Order		3.922	9.209	5.404	4.986	4.975
	L_∞	6.515e-3	6.277e-4	9.758e-7	1.477e-8	4.688e-10	1.491e-11
	Order		3.376	9.329	6.045	4.978	4.975

Table 6.2
Example 6.1: Solution errors with periodic boundary conditions, $t = 1.0$ and $\epsilon = 1$.

method	N	10	20	40	80	160	320
ADER-SHWENO	L^1	3.006e-3	1.977e-5	2.867e-7	1.929e-8	1.297e-9	8.404e-11
	Order		7.248	6.108	3.893	3.895	3.948
	L^2	4.339e-3	2.287e-5	3.195e-7	2.143e-8	1.441e-9	9.335e-11
	Order		7.568	6.162	3.898	3.895	3.948
	L_∞	7.043e-3	3.983e-5	4.563e-7	3.036e-8	2.038e-9	1.320e-10
	Order		7.466	6.448	3.910	3.897	3.948

Table 6.3
Example 6.2: Errors in computed density for periodic boundary conditions, $t = 1.0$ and $\mu = 0.0001$.

method	N	20	40	80	160	320
ADER-SHWENO	L^1	4.251e-4	1.243e-5	4.007e-7	1.253e-8	3.916e-10
	Order		5.096	4.955	4.999	4.999
	L^2	5.949e-3	1.403e-5	4.412e-7	1.382e-8	4.320e-10
	Order		5.406	4.991	4.997	5.000
	L_∞	9.998e-4	2.409e-5	6.344e-7	1.930e-8	6.023e-10
	Order		5.375	5.247	5.039	5.002

$$\partial_{tt}W = -\left(\frac{\partial^2 F}{\partial W^2}\partial_t W\right)\partial_x W - \frac{\partial F}{\partial W}\partial_{xt}W + \left(\frac{\partial^2 D}{\partial W^2}\partial_t W\right)\partial_x W\,\partial_x W + \left(\frac{\partial D}{\partial W}\partial_{xt}W\right)\partial_x W + \left(\frac{\partial D}{\partial W}\partial_x W\right)\partial_{xt}W + \left(\frac{\partial D}{\partial W}\partial_t W\right)\partial_{xx}W + D\partial_{xxt}W,$$

and so on. From these equations, we can observe that $\partial_t^{(k)}W$ is a function of $\partial_x W^{(2k)}$ now, which is different from the inviscid Euler equation. Moreover, $\partial_x W^{(2k)}(k > 2)$ is set to be 0 since the degree of the polynomial is four at most in this paper.

Finally, the cell average of the derivatives at the next time in Sec. 2.4 is now evaluated by

$$\bar{V}_j^{n+1} = \frac{1}{\Delta x}\int_{I_j} W_x(x, t_{n+1})dx = \frac{W(x^-_{j+\frac{1}{2}}, t_{n+1}) - W(x^-_{j-\frac{1}{2}}, t_{n+1})}{\Delta x}. \tag{6.11}$$

To demonstrate the performance of the ADER-SHWENO method, we test an example for the scalar linear advection-diffusion equation, and several examples for the Navier-Stokes equations in one dimension in the following section. In addition, to demonstrate the good performance, we also provide the comparison with the fifth order positivity-preserving finite volume hybrid Hermite WENO schemes [9], which is termed as PP-HWENO.

Example 6.1. First we consider the following linear advection-diffusion equation

$$W_t + W_x = \epsilon W_{xx},\ x \in (0, 2),$$

with the initial condition $W(x, 0) = \sin(\pi x)$ and a periodic boundary condition is applied at both ends.

The exact solution for this linear problem is $W(x, t) = e^{-\epsilon t}\sin(\pi(x - t))$. The errors with $\epsilon = 0.01$ and $\epsilon = 1$ at $t = 1$ are listed in Table 6.1 and Table 6.2, respectively. From the tables, one can observe that our method obtains the designed order of accuracy. Moreover, the fifth order is achieved when the convection is dominated and the order is decreased to four while the diffusion is dominated.

Example 6.2. In this example, we consider the one-dimensional compressible Navier-Stokes equation (6.1). To verify the accuracy of the ADER-SHWENO method for Navier-Stokes equation, the numerical example of the linear advection equation in Example 5.2 is extended to the viscous Navier-Stokes equation with the same initial condition and boundary condition. The parameters P_r and γ are taken as $\frac{2}{3}$ and 1.4, respectively.

Table 6.4
Example 6.2: Errors in computed density for periodic boundary conditions, $t = 1.0$ and $\mu = 0.1$.

method	N	20	40	80	160	320
ADER-SHWENO	L^1	1.533e-4	5.224e-6	1.885e-7	7.331e-9	3.188e-10
	Order		4.875	4.793	4.684	4.523
	L^2	1.643e-4	5.793e-6	2.139e-7	8.400e-9	3.665e-10
	Order		4.826	4.759	4.670	4.519
	L_∞	2.979e-4	1.144e-5	4.277e-7	1.686e-8	7.321e-10
	Order		4.703	4.741	4.665	4.525

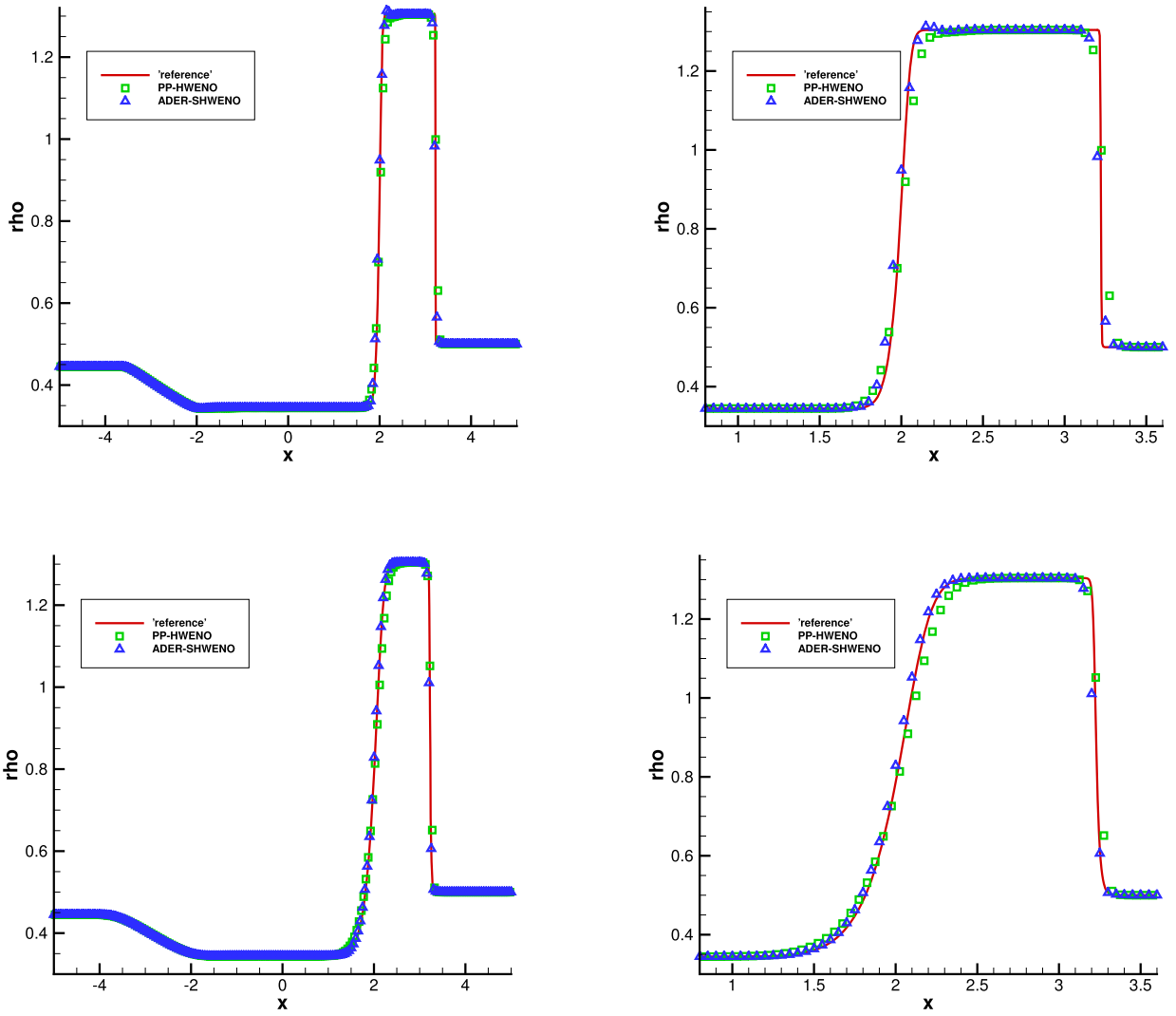

Fig. 6.1. Example 6.3: The density obtained by ADER-SHWENO method with $N = 200$ uniform meshes is compared with ones obtained by PP-HWENO method. Top: $\mu = 0.001$; Bottom: $\mu = 0.01$.

We compute the problem up to $t = 1$. Particularly, the numerical convergence rates are estimated by the asymptotic convergence error proposed in [36] since there are no exact solutions for this problem, which is also used in [4,34]. The errors and corresponding numerical orders with the different parameters $\mu = 0.0001$ and $\mu = 0.1$ are shown in Table 6.3 and Table 6.4, respectively. From the tables, it is observed that our method can obtain the designed order of accuracy. Moreover, it can achieve the fifth order when the advection is dominated, i.e., $\mu = 0.0001$, and the order is decreased while the diffusion is dominated, i.e., $\mu = 0.1$.

Example 6.3. The Lax problem in Example 5.3 is extended to the viscous Navier-Stokes equation (6.1). And the parameters P_r and γ are set to be 0.72 and 1.4, respectively. We set the same initial condition, boundary condition and computational domain as Example 5.3.

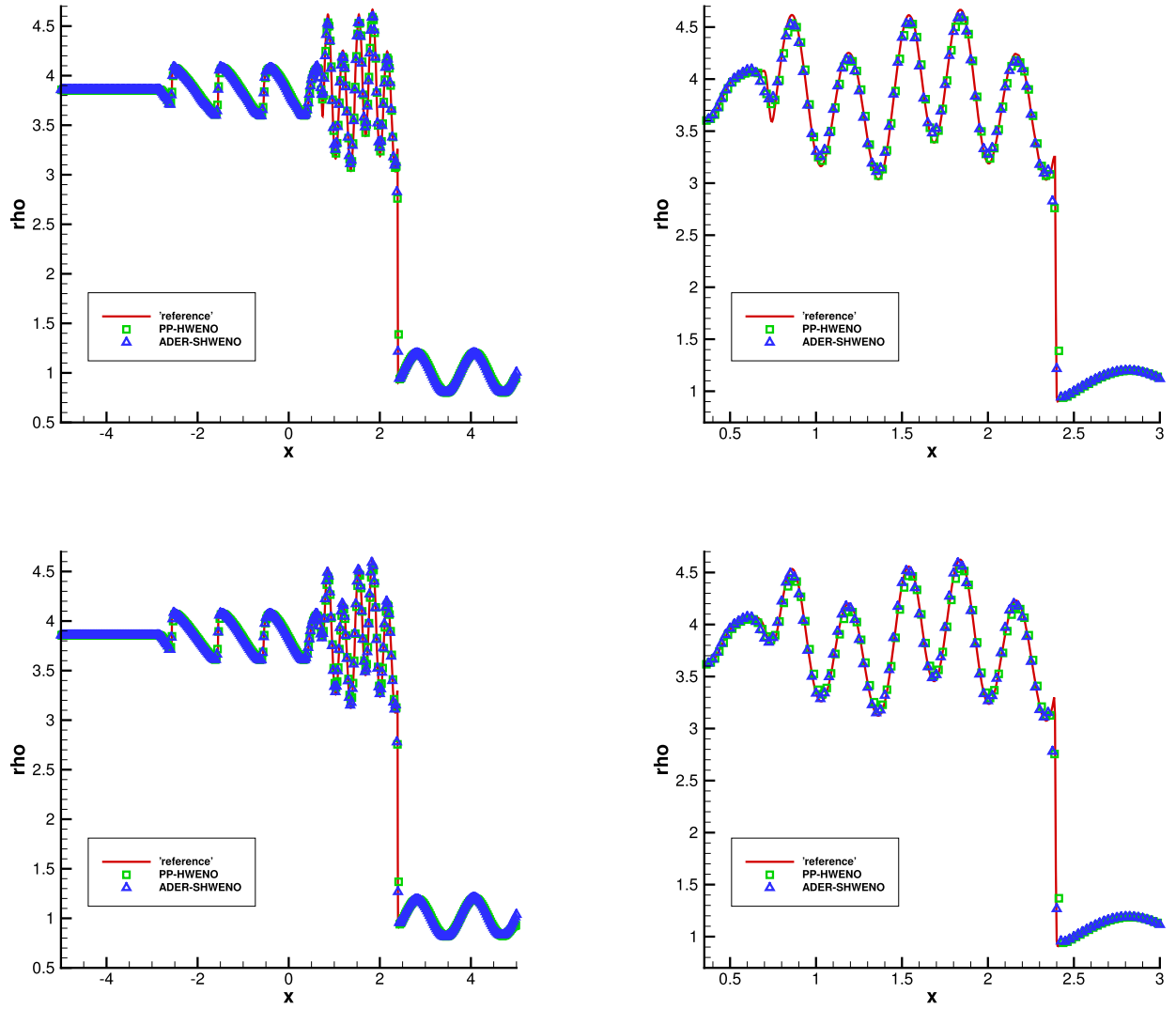

Fig. 6.2. Example 6.4: The density obtained by ADER-SHWENO method with $N = 400$ uniform meshes is compared with the ones obtained by PP-HWENO method. Top: $\mu = 0.0001$; Bottom: $\mu = 0.001$.

The results of the density obtained by the ADER-SHWENO and PP-HWENO method with $N = 200$ uniform meshes with $\mu = 0.001$ and $\mu = 0.01$ at time $t = 1.3$ are shown Fig. 6.1. The reference solution is obtained by the ADER-SHWENO method with 2000 uniform mesh points. From the figures, one can see that the contact discontinuity, and the front and the tail of the rarefaction wave are becoming smoother as the parameter μ is increased. In addition, the resolution of the result obtained by ADER-SHWENO method is clearly better than the results obtained by the PP-HWENO method in [9].

Example 6.4. The Shu-Osher problem in Example 5.4 is extended to the viscous Navier-Stokes equation (6.1). Thus, the initial condition, the computational domain, and the boundary condition are taken as Example 5.4. And the parameters P_r and γ are also set to be 0.72 and 1.4, respectively.

The results of the density obtained by the ADER-SHWENO method with $N = 400$ uniform meshes with $\mu = 0.0001$ and $\mu = 0.001$ at time $t = 1.8$ are compared with the solutions obtained by the PP-HWENO method in Fig. 6.2 against the reference solution obtained by the method with $N = 2000$ uniform meshes. From the figures, one can observe that our results are comparable with the ones obtained by PP-HWENO proposed in [9] for $\mu = 0.0001$ and a little better than the results with PP-HWENO method when $\mu = 0.001$.

Remark. From the figures, one may find that although the parameter μ is small and the advection is dominated, the resolution is lower than the results in Example 5.4 with the same number of points. The main reason is that the Lax-Friedrich flux is employed in this example instead of HLLC in Example 5.4. Besides, the order of the ADER-SHWENO method for the viscous Navier-Stokes equation is decreased to four.

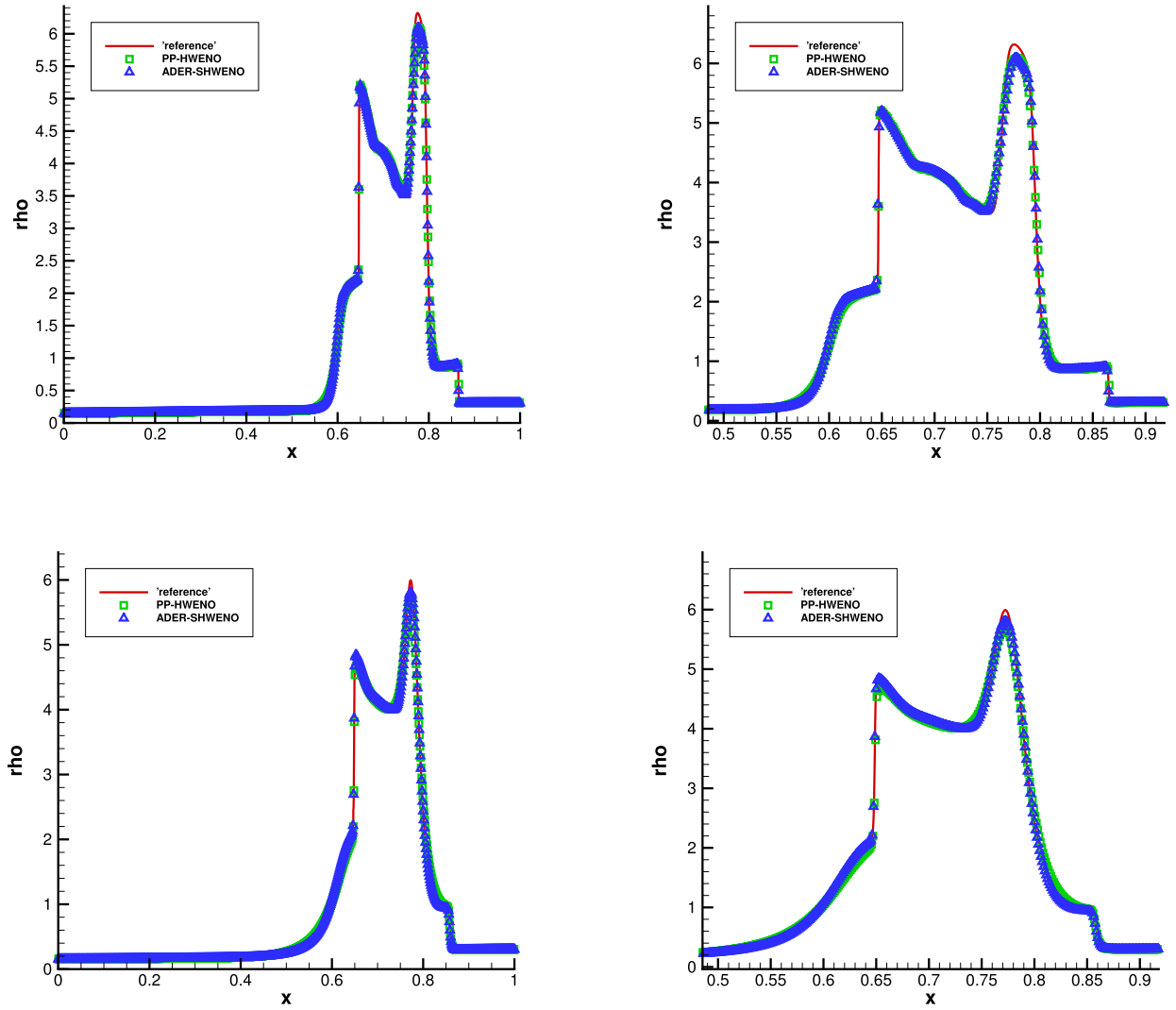

Fig. 6.3. Example 6.5: The density obtained by ADER-SHWENO method with $N = 800$ uniform meshes is compared with these obtained by PP-HWENO method. Top: $\mu = 0.001$; Bottom: $\mu = 0.01$.

Example 6.5. The interaction of blast waves of the viscous Navier-Stokes equation (6.1) is considered. The initial condition, the computational domain, and the boundary condition are the same as the Example 5.6. And the same parameters P_r and γ as Example 6.3 are taken.

The numerical solutions (density) obtained by both the ADER-SHWENO method and the PP-HWENO method with $N = 800$ uniform meshes with $\mu = 0.001$ and $\mu = 0.01$ at time $t = 0.038$ are plotted in Fig. 6.3, where the reference solution is obtained by the ADER-SHWENO method with 2000 uniform mesh points. From the figures, it is observed that our results are comparable with the ones obtained by the PP-HWENO method for $\mu = 0.001$ and is slightly better for $\mu = 0.01$, which is the same as Example 6.4.

References

[1] M. Castro, B. Costa, W.S. Don, High order weighted essentially non-oscillatory WENO-Z schemes for hyperbolic conservation laws, J. Comput. Phys. 230 (2011) 1766–1792.
[2] B. Cockburn, S.-Y. Lin, C.-W. Shu, TVB Runge-Kutta local projection discontinuous Galerkin finite element method for conservation laws III: one dimensional systems, J. Comput. Phys. 84 (1989) 90–113.
[3] B. Cockburn, C.-W. Shu, The Runge-Kutta discontinuous Galerkin method for conservation laws V: multidimensional systems, J. Comput. Phys. 141 (1998) 199–224.
[4] S. Cui, J. Zhu, A new finite volume multi-resolution central WENO scheme for Navier–Stokes equations on staggered meshes, Comput. Methods Appl. Mech. Eng. 393 (2022) 114822.
[5] M. Dumbser, Building blocks for arbitrary high order discontinuous Galerkin schemes, J. Sci. Comput. 27 (2006) 215–230.
[6] M. Dumbser, M. Käser, Arbitrary high order non-oscillatory finite volume schemes on unstructured meshes for linear hyperbolic systems, J. Comput. Phys. 221 (2007) 693–723.

[7] M. Dumbser, M. Käser, V.A. Titarev, E.F. Toro, Quadrature-free non-oscillatory finite volume schemes on unstructured meshes for nonlinear hyperbolic systems, J. Comput. Phys. 226 (2007) 204–243.
[8] F. Fambri, M. Dumbser, O. Zanotti, Space-time adaptive ADER-DG schemes for dissipative flows: compressible Navier-Stokes and resistive MHD equations, Comput. Phys. Commun. 220 (2017) 297–318.
[9] C. Fan, X. Zhang, J. Qiu, Positivity-preserving high order finite volume hybrid Hermite WENO schemes for compressible Navier-Stokes equations, J. Comput. Phys. 445 (2021) 110596.
[10] Y. Gu, G. Hu, A third order adaptive ADER scheme for one dimensional conservation laws, Commun. Comput. Phys. 22 (2017) 829–851.
[11] A. Harten, B. Engquist, S. Osher, S.R. Chakravarthy, Uniformly high order accurate essentially non-oscillatory schemes III, J. Comput. Phys. 71 (1987) 231–303.
[12] G.S. Jiang, C.-W. Shu, Efficient implementation of weighted ENO schemes, J. Comput. Phys. 126 (1996) 202–228.
[13] P.D. Lax, X.-D. Liu, Solutions of two-dimensional Riemann problems of gas dynamics by positive schemes, SIAM J. Sci. Comput. 19 (1998) 319–340.
[14] D. Levy, G. Puppo, G. Russo, Central WENO schemes for hyperbolic systems of conservation laws, Math. Model. Numer. Anal. 33 (1999) 547–571.
[15] D. Levy, G. Puppo, G. Russo, Compact central WENO schemes for multidimensional conservation laws, SIAM J. Sci. Comput. 22 (2000) 656–672.
[16] S. Li, Y. Chen, S. Jiang, An efficient high-order gas-kinetic scheme (I): Euler equations, J. Comput. Phys. 415 (2020) 109488.
[17] S. Li, D. Luo, J. Qiu, Y. Chen, A compact and efficient high-order gas-kinetic scheme, J. Comput. Phys. 447 (2021) 110661.
[18] N. Liu, H. Tang, A high-order accurate gas-kinetic scheme for one- and two-dimensional flow simulation, Commun. Comput. Phys. 15 (2014) 911–943.
[19] D. Luo, W. Huang, J. Qiu, A quasi-Lagrangian moving mesh discontinuous Galerkin method for hyperbolic conservation laws, J. Comput. Phys. 396 (2019) 544–578.
[20] D. Luo, W. Huang, J. Qiu, A hybrid LDG-HWENO scheme for KdV-type equations, J. Comput. Phys. 313 (2016) 754–774.
[21] J. Qiu, C.-W. Shu, Finite difference WENO schemes with Lax-Wendroff-type time discretizations, SIAM J. Sci. Comput. 24 (2003) 2185–2198.
[22] J. Qiu, C.-W. Shu, Hermite WENO schemes and their application as limiters for Runge-Kutta discontinuous Galerkin method: one dimensional case, J. Comput. Phys. 193 (2004) 115–135.
[23] J. Qiu, C.-W. Shu, Hermite WENO schemes and their application as limiters for Runge-Kutta discontinuous Galerkin method II: two dimensional case, Comput. Fluids 34 (2005) 642–663.
[24] J. Qiu, Hermite WENO schemes with Lax-Wendroff type time discretizations for Hamilton-Jacobi equations, J. Comput. Math. 25 (2007) 131–144.
[25] J. Qiu, M. Dumbser, C.-W. Shu, The discontinuous Galerkin method with Lax-Wendroff type time discretizations, Comput. Methods Appl. Mech. Eng. 194 (2005) 4528–4543.
[26] X. Ren, K. Xu, W. Shyy, C. Gu, A multi-dimensional high order discontinuous Galerkin method based on gas kinetic theory for viscous flow computations, J. Comput. Phys. 292 (2015) 176–193.
[27] C.-W. Shu, Total-variation-diminishing time discretizations, SIAM J. Sci. Stat. Comput. 9 (1988) 1073–1084.
[28] V.A. Titarev, E.F. Toro, ADER: arbitrary high order Godunov approach, J. Sci. Comput. 17 (2002) 609–618.
[29] V.A. Titarev, E.F. Toro, ADER schemes for three-dimensional non–linear hyperbolic systems, J. Comput. Phys. 204 (2005) 715–736.
[30] E.F. Toro, Riemann Solvers and Numerical Methods for Fluid Dynamics: A Practical Introduction, Springer-Verlag, Berlin, Heidelberg, 2009.
[31] E.F. Toro, V.A. Titarev, Derivative Riemann solvers for systems of conservation laws and ADER methods, J. Comput. Phys. 212 (2006) 150–165.
[32] E.F. Toro, V.A. Titarev, TVD fluxes for the high-order ADER schemes, J. Sci. Comput. 24 (2005) 285–309.
[33] E.F. Toro, R.C. Millington, L.A.M. Nejad, Towards very high-order Godunov schemes, in: Godunov Methods: Theory and Applications. Edited Review, Kluwer Academic/Plenumm Publishers, 2001, pp. 905–937.
[34] Z. Wang, J. Zhu, L. Tian, N. Zhao, A low dissipation finite difference nested multi-resolution WENO scheme for Euler/Navier-Stokes equations, J. Comput. Phys. 429 (2021) 110006.
[35] P.R. Woodward, P. Colella, The numerical simulation of two-dimensional fluid flow with strong shocks, J. Comput. Phys. 54 (1984) 115–173.
[36] Y.-T. Zhang, J. Shi, C.-W. Shu, Y. Zhou, Numerical viscosity and resolution of high-order weighted essentially nonoscillatory schemes for compressible flows with high Reynolds numbers, Phys. Rev. E 68 (2003) 046709.
[37] Z. Zhao, Y. Chen, J. Qiu, A hybrid Hermite WENO scheme for hyperbolic conservation laws, J. Comput. Phys. 405 (2020) 109175.
[38] J. Zhu, J. Qiu, A new fifth order finite difference WENO schemes for solving hyperbolic conservation laws, J. Comput. Phys. 318 (2016) 110–121.
[39] J. Zhu, J. Qiu, A new type of finite volume WENO schemes for hyperbolic conservation laws, J. Sci. Comput. 73 (2017) 1338–1359.
[40] J. Zhu, J. Qiu, Hermite WENO schemes and their application as limiters for Runge-Kutta discontinuous Galerkin method, III: unstructured meshes, J. Sci. Comput. 39 (2009) 293–321.